An International Journal of Optimization and Control: Theories & Applications
ISSN: 2146-0957 eISSN: 2146-5703
Vol.15, No.4, pp.625-648 (2025)
https://doi.org/10.36922/IJOCTA025150076

RESEARCH ARTICLE

Advanced frequency control strategy for power systems with high renewable energy penetration: A battery energy storage system approach

Tran Viet Thanh[1], Le Cao Quyen[2], Dinh Thanh Viet[3], Nguyen Huu Hieu[1], and Le Van Dai[2*]

[1]Power Systems Department, Faculty of Electrical Engineering, University of Science and Technology - University of Da Nang, Da Nang, Vietnam
[2]Electric Power System Research Group, Faculty of Electrical Engineering Technology, Industrial University of Ho Chi Minh City, Ho Chi Minh, Vietnam
[3]Department of Electrical and Electronic Engineering, Faculty of Electrical and Electronic Engineering, Dong A University, Da Nang, Vietnam
levandai@iuh.edu.vn, thanh.tv@pecc4.vn, quyen.lc@pecc4.vn, vietdt@donga.edu.vn, nhhieu@dut.udn.vn

ARTICLE INFO

Article History:
Received: April 9, 2025
Revised: June 22, 2025
Accepted: July 3, 2025
Published Online: August 11, 2025

Keywords:
Adaptive nonlinear droop control
Battery energy storage system
Frequency stability
Rate of change of frequency
Renewable energy sources
State of charge

AMS Classification 2010:
90B23, 90B56

ABSTRACT

This study proposes an optimal control strategy for battery energy storage systems to support frequency regulation in power systems with high renewable energy penetration. The algorithm generates a sinusoidal reference signal for the pulse-width modulation scheme of the direct current/alternating current converter, adjusting it based on voltage magnitude and phase set points. The control system integrates multiple loops to manage frequency, voltage, active and reactive powers, charge, and current controllers on the d- and q-axes. It limits frequency deviations and improves the rate of change of frequency. An adaptive nonlinear droop control method, combined with state-of-charge (SOC) feedback, regulates active power-frequency control to enhance grid stability. The SOC feedback mechanism enables dynamic charge and discharge operations, ensuring that frequency remains within operational limits. Simulation results, validated using modified Vietnamese Tay Nguyen 500/220 kV and IEEE 39-bus systems with DIgSILENT/PowerFactory, show that the proposed method outperforms the conventional CBEST model in scenarios involving sudden generation outages or fluctuating renewable energy output. This method meets the frequency stability requirements set by the Circular No. 25/2016/TT-BCT of the Vietnamese Ministry of Industry and Trade, ensuring that the system operates within a stable frequency range of 49.5–50.5 Hz under 120 s and recovers to 49.8–50.2 Hz within 300 s.

1. Introduction

The future of electricity generation lies in renewable energy sources (RESs). Among these, solar photovoltaic and wind power are the most significant and promising due to their inexhaustibility, cleanliness, and global accessibility. Many countries are focusing on the rigorous implementation of RES-based output goals, reducing greenhouse gas emissions, and decreasing reliance on oil and coal. With the increasing urgency of addressing climate change, nations worldwide are transitioning to renewable energy to protect the environment. Over the past decade, wind and solar energy have seen substantial growth and are now top priorities in energy planning.

For instance, in 2023, Germany generated around 40% of its electricity from renewable sources, with wind energy playing a significant

*Corresponding Author

role. This is supported by reports from the German Federal Ministry for Economic Affairs and Energy. According to the National Energy Administration, in 2023, renewable energy accounted for approximately 30% of China's total electricity capacity, with substantial contributions from both wind and solar power. In the United States, RESs contributed about 20% of total electricity production, as reported by the United States Energy Information Administration. In Denmark, over 50% of electricity was generated from wind energy in 2022, according to the Danish Energy Agency. In Spain, wind and solar energy together contributed about 30% to total electricity production. India aimed to achieve 175 GW of renewable energy capacity in 2022, including 100 GW from solar and 60 GW from wind, as reported by the Spanish grid operator Red Eléctrica de España. In Turkey, the total electricity capacity reached 97.7 GW, with over 53% of it generated by RESs.[1]

As the adoption of solar photovoltaic and wind energy increases, the reliance on fossil fuels for electricity generation decreases, bringing both economic and ecological benefits. However, there are significant challenges and risks due to the ongoing reconfiguration of power system operations. Consequently, the power system faces stability challenges. Many of these RESs do not provide the same inertia as synchronous generators, which reduces the system's ability to maintain frequency stability after a fault. Additionally, these sources may struggle to provide stable reactive power, weakening voltage stability, and leading to potential voltage problems. Furthermore, the output from these renewable sources is weather-dependent, causing fluctuations in power generation and complicating prediction and control. The integration of multiple renewable sources also requires more complex management and control systems to ensure coordination and optimization across the entire power system.

A typical example of frequency fluctuations caused by a generation outage of up to 1800 MW is shown in Figure 1.[2] The rate of change of frequency (RoCoF) represents how quickly the frequency drops. RoCoF is directly proportional to the disturbance and inversely proportional to the system's inertia constant. Maintaining the load frequency at its nominal value is crucial to ensuring the safe and reliable operation of the power system. Frequency regulation is achieved through primary frequency control (PFC), secondary frequency control, and tertiary frequency control loops, depending on the frequency deviation range. The PFC is a rapid-response control loop that operates in the first 30 s after a disturbance.[3] It is automatically provided by the inertia of synchronous generators and motors directly connected to the grid, which resist sudden frequency changes. This control is also supported by the speed governor systems. The secondary frequency control follows the PFC when a large frequency deviation persists for a longer period, typically between 30 and 1800 s. It is provided by automatic generation control and manual actions.[4] The tertiary frequency control is an emergency control strategy that must be implemented if the frequency drops below the required threshold after a significant event. It requires an optimal solution to restore stability.[5] Therefore, each stage corresponds to different time scales and transient phenomena, each requiring specific support measures.

Wind and solar power plants use inverters, which lack the inertia characteristic of synchronous generators. The variability of wind and solar resources complicates the maintenance of supply-demand balance. Wind turbines, in particular, may experience higher errors when tracking the voltage phase angle during faults, further complicating frequency regulation and stabilization. Traditionally, frequency control in systems with integrated renewable RESs has relied on thermal and hydropower plants.[6] However, when a substantial amount of renewable energy and power electronic equipment are integrated into the grid, the power system exhibits weak damping and low inertia, making it difficult to maintain frequency stability.[7] As a result, this conventional approach becomes less effective, leading to frequency fluctuations that fall outside the permissible network frequency range.[8]

Battery energy storage systems (BESS) are essential technologies for energy management and storage and are increasingly being proposed as a key alternative for frequency stabilization. In addition to the numerous benefits of BESS, such as enhancing frequency dynamics performance,[9] storing, and releasing energy over short periods,[10] improving grid stability, reducing energy costs, and providing backup power,[11] and selecting the appropriate control method remains a significant challenge. Numerous studies have focused on integrating BESS with existing synchronous generators to support automatic generation control (AGC) and restore system frequency to its nominal value. For example, Xie et al.[12] proposed the model predictive control method to optimize BESS operation. The study presented experimental or simulation results demonstrating that using BESS in AGC systems can greatly enhance

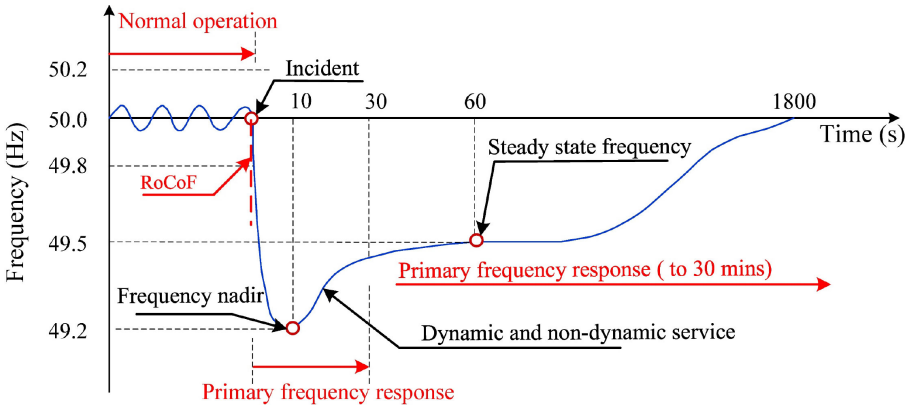

Figure 1. Frequency fluctuations resulting from a generation outage of up to 1800 MW. Adapted from Teng et al.[2]
Abbreviation: RoCoF, rate of change of frequency.

grid frequency stability and improve the operational efficiency of coal-fired thermal power plants in China. Beyond China, BESS is also deployed as an auxiliary service, including AGC, in power systems across countries such as Denmark, Japan, and in some parts of Africa.[13–15]

In recent years, BESS has been deployed and installed at various locations within the grid for support applications. Among these, frequency support for wind and photovoltaic (PV) systems has been widely discussed due to their fast response and high ramp rate. Gulzar et al.[16] introduced a BESS that balances energy and stabilizes frequency in hybrid PV, wind, and fuel-cell systems. The BESS is controlled using the proportional-integral (PI) method. Taghvaei et al.[17] also proposed the PI method to control the BESS and improve the frequency stability of large-scale PV and wind farms. In the study, the authors use the Particle Swarm Optimization-fuzzy method to tune the main parameters of the PI controller. While this method enhances control performance, it increases computational complexity, leading to delays in the response of large real-time operating systems and affecting the transient response of the BESS during frequency regulation. A control algorithm based on adjustable state-of-charge (SOC) limits was developed by Mercier et al.[18] However, this approach combines BESS sizing optimization without addressing the determination of optimal SOC limits. To the best of the authors' knowledge, BESS sizing optimization is typically based on predefined conditions, but sudden changes in load or renewable energy output are highly unpredictable. An adaptive synthetic inertia control based on the voltage source converter for primary frequency control of the BESS was proposed by Gu et al.[19] to enhance system frequency stability. However, the study only considered a power system with wind energy and a simple grid, making the method less applicable to complex grids with multiple energy sources due to factors such as latency, noise, and complex operational conditions. Islam et al.[20] introduced a frequency control method for the BESS based on available PV power in the network. These approaches centralize the frequency stability of the system, particularly in systems with wind or PV energy, by controlling the BESS.

Several studies have been conducted on the operation and optimization of BESS grid connections.[21–25] El-Bidairi et al.[21] developed a method based on the grey wolf optimizer to determine the optimal BESS size. This technique is centralized to examine the worst-case growth in frequency fluctuations in electrical generation and consumption. However, the algorithm requires significant computation, especially for complex systems with many variables, making it difficult to deploy on a large scale or in real-time operating systems. A multi-objective evaluation method was proposed by Teh et al.[22] to optimize BESS capacity. While the algorithm is highly effective, it has not been applied to real-world power grid scenarios, which could limit its applicability under different operating conditions. A BESS model was developed using Python and OpenDSS to improve operational efficiency and economic benefits in low-voltage grids.[23] Although this model aimed to optimize economic benefits, its ability to integrate with complex economic models, such as electricity price simulations, energy policies, and market factors, may be constrained in Python and OpenDSS without appropriate tools or data. The meta-heuristic artificial bee colony (ABC) algorithm was used to optimize BESS size and minimize frequency deviation by Das et al.[24] Like

other swarm algorithms, the ABC method can become trapped in local optima rather than finding the global optimum, leading to suboptimal BESS sizing. Additionally, the algorithm is highly sensitive to input parameters, and incorrect adjustments can adversely affect the optimization results. Alsharif et al.[25] proposed an alternative method for determining the size and placement of the BESS to maintain frequency stability in relation to system generation and demand was proposed. However, this method assumes the internal resistance of the BESS and batteries to be constant, whereas, in reality, these parameters vary with SOC and temperature. Furthermore, the method is only applicable to the IEEE 39-bus grid.

As discussed in some related works above, the impact of uncertainties related to generation output, load, and intermittent generation sources has been considered. BESS devices are proposed to improve frequency stability; however, existing approaches mainly focus on determining optimal location and capacity. This article introduces a new algorithm that utilizes voltage magnitude and phase set points through control loops, including frequency, voltage, reactive and active powers, charge, and d- and q-axes current controllers for the BESS. The proposed method improves frequency stability and controls the power flow on inter-domain transmission lines under various conditions and adverse situations in the grid by integrating multiple RESs. From the authors' perspective, this issue has not been fully addressed in the literature. The main contributions of this method are summarized as follows.

(i) A detailed analysis of the impact of BESS in supporting frequency regulation in power systems with a high penetration rate of RESs.
(ii) Modeling the BESS as a storage system with a direct current (DC)/alternating current (AC) converter that can replace the existing synchronous generators to accommodate the increasing penetration of wind and PV units.
(iii) Proposing the BESS system to provide primary frequency control by supplying stored power to the grid during disturbances (such as cloud cover, generator tripping, or power output shortages), while also acting as a secondary frequency controller by absorbing excess power to reduce grid frequency and restore its initial energy level.
(iv) Proposing a solution to use BESS equipment to improve frequency stability and ensure compliance with the conditions set by Circular No. 25/2016/TT-BCT, dated November 30, 2016, from the Ministry of Industry and Trade of Vietnam, regulating transmission power systems.

The remainder of this paper is organized as follows: Section 2 presents the theoretical foundation of the problem and the basis for developing the proposed method. Section 3 outlines the details of the proposed control strategy for the BESS. Section 4 provides an analysis and interpretation of the simulation results for the test systems used. Finally, Section 5 provides the conclusion of this paper.

2. Formulation of the problem

Figure 2 shows the generalized load frequency control for the power system in which the RESs and BESS are connected. The parameters are denoted as mathematical symbols and defined as follows: P_{G_i} is the generating power of the ith generator G_n, $\sum P_L$ is the sum of load power, P_{BESS} is the BESS power, $\sum H$ is the sum of the inertia constant of all rotating machines, including wind turbines, f_{ref} is the reference frequency, f_{s} is the system frequency, D_i is the nth droop coefficient of the ith generation system G_i, H_{BESS} is the droop coefficient of the BESS, and $P_{wind+\text{PV}}$ is the sum of the generated power of all RESs, including the generated sources of wind and PV, and can be determined as follows[26,27] in Equation (1):

$$P_{wind+PV} = \underbrace{\frac{1}{2}\rho A_w v^3 C_p}_{P_{wind}} + \underbrace{\eta A_{PV} G}_{P_{PV}} \tag{1}$$

where P_{wind} is the wind power, P_{PV} is the solar power, ρ is the air density, v is the wind speed, A_w is the swept area of the blades, C_p is the power coefficient, η is the efficiency of the solar panel, A_{PV} is the area of the solar panel, and G is the solar irradiance.

The impact of RESs on the power system frequency refers to the effects that variable RESs, such as wind and solar power, can have on the balance between power generation and consumption in an electrical grid. When the power output from RESs fluctuates, it can cause variations in the grid frequency. This is because RESs like wind and solar power are intermittent and variable, meaning their output can change rapidly due to changes in weather conditions. The impact of RESs on power system frequency can be significant, particularly if the grid is not designed to handle the variability of these sources. This impact can be assessed as follows in Equation (2).

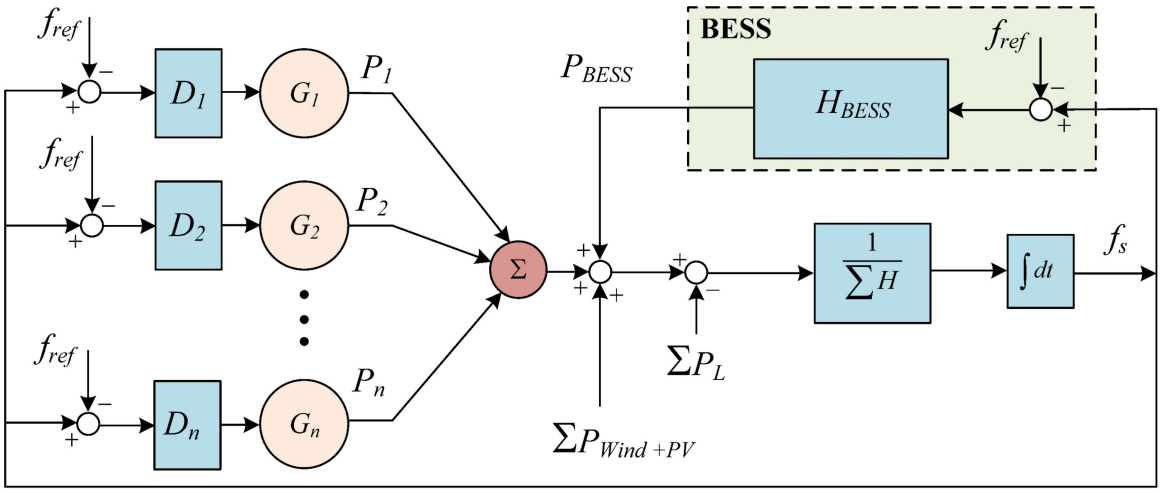

Figure 2. Frequency response method of the power system considering the fluctuation of the renewable energy source power
Abbreviation: BEES: Battery energy storage system.

$$\Delta f = -\left(\frac{\Delta P}{2HS}\right) \tag{2}$$

in which Δf is the frequency deviation, which is the change in the power system's frequency when there is a change in power, ΔP is the power deviation, which refers to the difference between the generated power and the consumed power, including changes in power from wind and solar sources, H is the system inertia constant, a quantity that reflects the power system's ability to resist frequency changes, depending on the characteristics of the generators and loads, and S is the system's rated power, which is the maximum stable power that the power system can supply. This equation illustrates the relationship between power changes and frequency variations in the power system. When the generated power and consumed power are not balanced, the system frequency will fluctuate. A system with high inertia will be better able to resist frequency changes.

The system frequency must always remain within the allowable range under varying load conditions, which requires generators to temporarily compensate for any deviation by using their stored kinetic energy. The frequency response of the power system from the governor of the ith generator, considering the connected RESs, can be defined as follows in Equation (3)[28]:

$$\frac{df_s}{dt} = \frac{f_{\text{ref}}}{2\sum H}\left(\sum_{i=1}^{n} P_{G_i} - \sum P_L + \sum P_{wind+PV}\right) \tag{3}$$

From Equation (3), it can be seen that the grid frequency will fluctuate due to the constantly changing output of RESs. This can lead to an unstable electrical system due to irregular power supplies, potentially damaging equipment, causing interruptions, and even resulting in power outages. To mitigate the impact of RESs, it is essential to find technological solutions that maintain stability and enhance grid reliability. The BESS device offers an ideal solution. It can store excess energy from RESs and supply it to the grid when RES power is low, helping to stabilize grid frequency. When the BESS is connected to the power grid, the grid frequency response from the rotor dynamic equation is given as follows in Equation (4):

$$\frac{df_s}{dt} = \frac{f_{\text{ref}}}{H_{\text{BESS}} + 2\sum H} \times \left(P_{\text{BESS}} + \sum_{i=1}^{n} P_{G_i} - \sum P_L + \sum P_{wind+PV}\right) \tag{4}$$

where H_{BESS} is the inertial constant of the BESS that demonstrates the ability to respond when controlling the frequency. When the BESS is applied to provide inertial support during frequency fluctuations, its required reference power is adjusted according to the system's response capacity. It can be evaluated as given in Equation (5),[29] in which $P_{\text{BESS}}^{\text{ref\_1}}$ and $P_{\text{BESS}}^{\text{ref\_0}}$ are the reference powers with and without controlling the frequency, respectively.

$$P_{\text{BESS}}^{\text{ref\_1}} = P_{\text{BESS}}^{\text{ref\_0}} H_{\text{BESS}} f_s \frac{df_s}{dt} \tag{5}$$

The BESS is used to store excess energy from RESs and release this energy when needed to reduce the frequency fluctuations. However, the performance of the BESS depends on the control strategy. The detailed model and controller of the BESS are discussed in the next section.

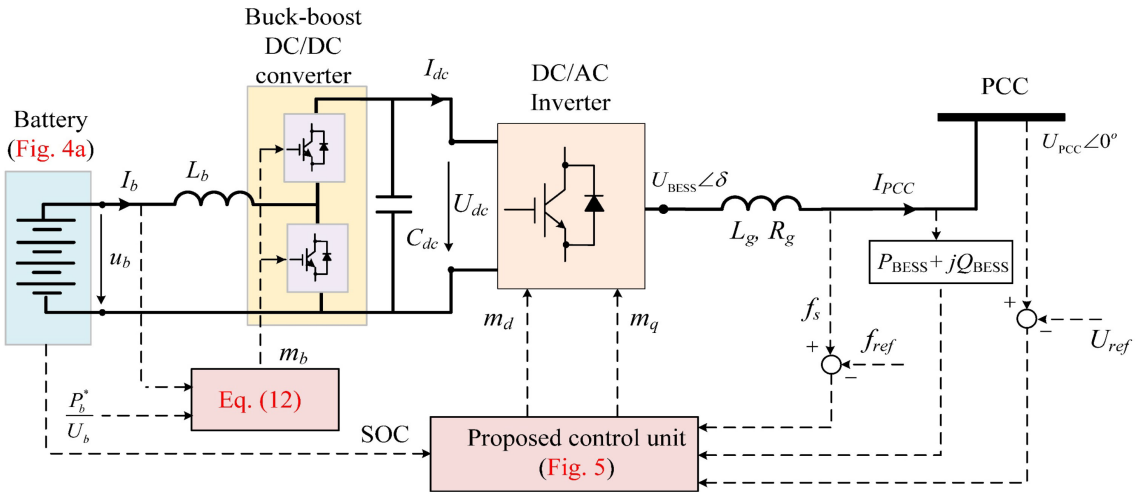

Figure 3. The structure and control strategy of the battery energy storage system (BEES)
Abbreviations: AC: Alternating current; DC: Direct current; SOC: State-of-charge.

For the frequency response model of the BESS, the structure and control strategy of the BESS in this study are detailed in Figure 3, including a battery energy storage system, buck-boost DC/DC converter, three-phase AD/AC inverter, and control system.

2.1. Mathematical modeling of the battery energy storage

The lithium-ion battery model for the proposed BESS is illustrated in Figure 4.[30] Figure 4a shows the topology using a controlled voltage source. This model assumes that the charging and discharging cycles exhibit similar characteristics. The typical characteristics for both charging and discharging are presented in Figure 4b and **c**, respectively. The output of the terminal voltage is calculated as follows in Equations (6) and (7).

$$u_b = u_{ch} - R_b i_b \tag{6}$$

$$u_b = u_{disch} - R_b i_b \tag{7}$$

where R_b is the internal resistance of the battery, i_b is the battery current, and u_{oc} is the voltage source that is primarily determined by the actual SOC of the battery, while also being influenced by other factors such as polarization. In MathWorks,[30] a general method for determining this voltage source has been proposed and validated by comparing the model with actual batteries. The calculation is determined under the charge and discharge models. For the charging model (sel = 1 in Figure 4a) with the condition $i_{l\_f} < 0$ and for the discharging model (sel = 1 in Figure 4a) with the condition $i_{l\_f} < 0$, the obtained battery voltage under the discharge and charge models can be expressed by Equations (8) and

$$u_{oc\_ch} = \left(u_0 - k\left(\frac{Q}{\int i_b dt + 0.1Q}\right) i_{l\_f} - k\left(\frac{Q}{Q - \int i_b dt}\right)\int i_b dt + Ae^{(-B\int i_b dt)}\right. \tag{8}$$

$$u_{oc\_disch} = \left(u_0 - k\left(\frac{Q}{Q - \int i_b dt}\right) i_{l\_f} - k\left(\frac{Q}{Q - \int i_b dt}\right)\int i_b dt + Ae^{(-B\int i_b dt)}\right. \tag{9}$$

where u_0 is the battery a constant voltage, k is the polarization constant, Q is the maximum capacity, i_{l_f} is the low-frequency current dynamics, A is the exponential voltage, B is the exponential capacity, and R_b is the internal resistance of the battery.

The value of the SOC is determined by applying the most common ampere-hour method as follows in Equation (10).

$$SOC = 1 - \int \frac{i_b t}{Q} dt \tag{10}$$

2.2. Direct current/direct current converter

The buck-boost DC/DC converter is used as a bidirectional power converter. It is designed to regulate the battery's output voltage, which varies according to the SOC. Charging power is applied when the buck converter is active, and discharging occurs when the boost converter is used. The current control method is employed to manage the charging and discharging of the battery.

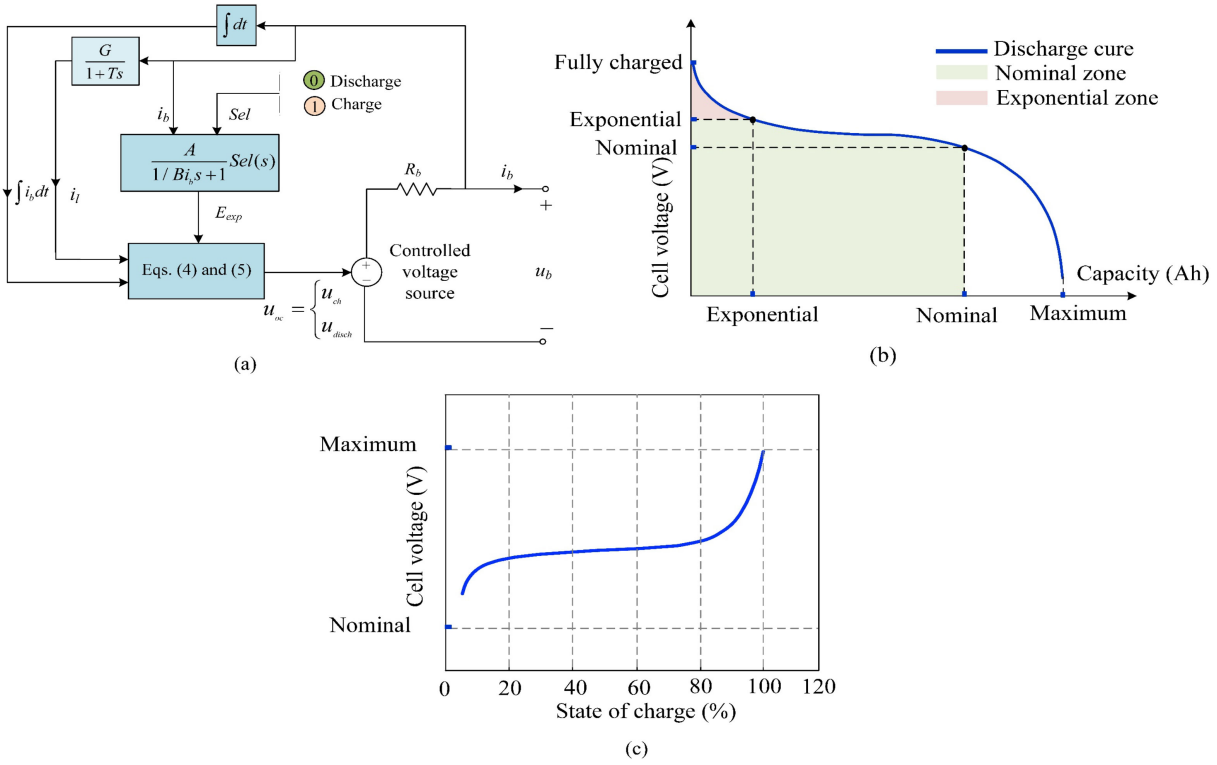

Figure 4. The battery model. (a) Equivalent model, (b) typical charge characteristics, and (c) typical discharge characteristics.

The injected power to the DC-link is as follows in Equation (11)[31]:

$$P_b = m_b U_{dc} I_b \tag{11}$$

in which, m_b is the duty cycle and can be determined as follows in Equation (12).

$$m_b = K_{p\_b}\left(\frac{P_b^*}{U_b} - I_b\right) + K_{i\_b}\int\left(\frac{P_b^*}{U_b} - I_b\right)dt \tag{12}$$

where P_b^* is the reference value injected into the power of the DC-link, and K_{p_b} and K_{i_b} are the proportional gain and integral time constant, respectively.

2.3. Direct current/alternating current converter

The DC/AC converter is used in the BESS to interface between the buck-boost DC/DC converter and the grid through the AC filter. In this paper, the DC/AC converter is implemented as a voltage source converter (VSC), which generates an AC voltage from a DC source. Typically, the VSC uses six insulated-gate bipolar transistors, which operate based on pulse-width modulation (PWM) with switching control. These insulated-gate bipolar transistors are usually controlled through PWM to regulate power flow. The active and reactive power delivered from the DC/AC converter to the grid can be obtained as follows in Equation (13)[32]:

$$\begin{cases} P_{\text{BESS}} = \left(\frac{U_{\text{BESS}}U_{PCC}}{Z_f}\cos\delta - \frac{U_{PCC}^2}{Z_f}\right)\cos\theta_g \\ \quad + \frac{U_{\text{BESS}}U_{PCC}}{Z_f}\sin\delta\sin\theta_f \\ Q_{\text{BESS}} = \left(\frac{U_{\text{BESS}}U_{PCC}}{Z_f}\cos\delta - \frac{U_{PCC}^2}{Z_f}\right)\sin\theta_g \\ \quad - \frac{U_{\text{BESS}}U_{PCC}}{Z_f}\sin\delta\cos\theta_f \end{cases} \tag{13}$$

where U_{BESS} is the output voltage of VSC, U_{PCC} is the voltage at the point of common coupling (PCC), δ is the power angle, Z_f is the filter impedance and is defined as $Z_f = R_f + jX_f$, θ_g is the impedance angle, R_f is the filter resistance, and X_f is the filter reactance and is considered based on the filter inductance L_f.

3. Proposed control

To enhance the frequency stability of the system, the converter control strategy for the BESS was considered in this work, as shown in Figure 5. This control system provided the voltage magnitude and phase set points to generate a sinusoidal reference signal for the PWM scheme of the DC/AC converter. The voltage magnitude and phase set points were determined using the reference voltage and frequency, which were derived through the outer and inner control loops. For frequency stability, the BESS was used to support active power. Therefore, the d-axis reference was

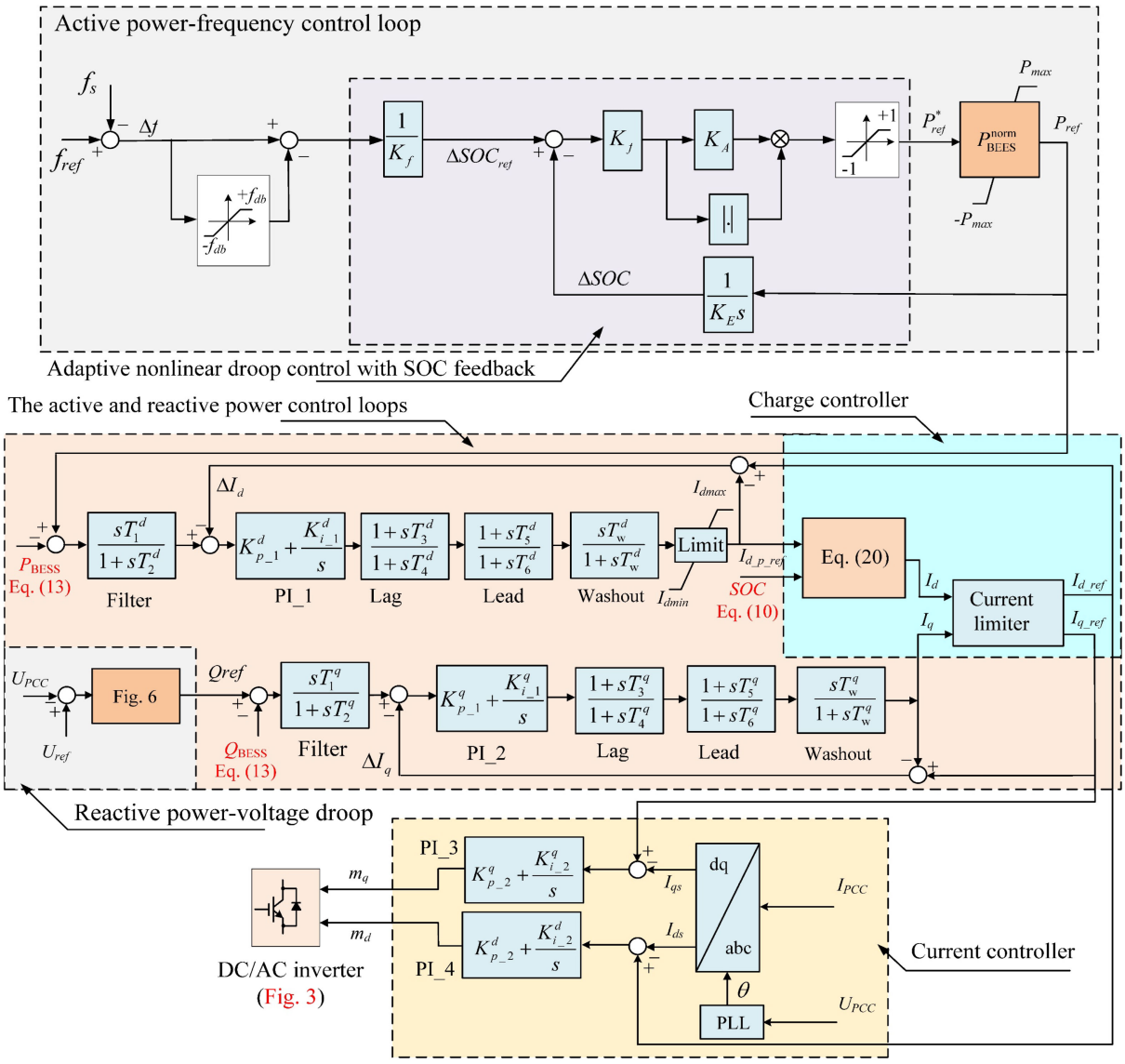

Figure 5. The proposed detailed control technique for the battery energy storage system

designed to regulate frequency, while the q-axis reference was designed to regulate voltage. The overall structure of the controller is organized into the following segments.

3.1. Active power-frequency droop control

As seen from Equation (3), the system inertia decreases when a power-frequency drop occurs, leading to instability in the power system. The adaptive nonlinear droop control with SOC feedback strategy was used to determine the nonlinear droop reference power of the converter based on the frequency error between the grid and the nominal frequency. Its value is as follows in Equation (14):

$$P^*_{\text{ref}} = \left(\left(\underbrace{f_{\text{ref}} - f_s}_{\Delta f} \right) \cdot \frac{1}{K_f} - P_{\text{ref}} \cdot \frac{1}{K_E s} \right) K_f K_r \quad (14)$$

From Equation (14), we obtained the transfer function of the reference power to the BESS in response to the frequency deviation, as defined in Equation (15). This transfer function is represented as a first-order low-pass filter.

$$\frac{P_{ref}}{\Delta f} = \frac{K_r P^{\text{norm}}_{\text{BESS}}}{1 + \frac{K_f K_r P^{\text{norm}}_{\text{BESS}}}{K_E s}} \quad (15)$$

where $P^{\text{norm}}_{\text{BESS}}$ is the rated power of the BESS, K_E is the BESS storage capacity, Δf is the frequency deviation between the reference frequency f_{ref} and the grid frequency f_s, and K_f is the conversion coefficient between the SOC and the grid frequency for the SOC feedback, and is defined as follows in Equation (16):

$$K_f = \frac{f_{ofs,max} - f_{ofs,min}}{SOC_{tot}} \quad (16)$$

in which $f_{ofs,max}$ and $f_{ofs,min}$ are the maximum and minimum offset frequencies, respectively. SOC_{tot} is the SOC control range, and K_r is the primary droop gain and can be expressed as follows in Equation (17):

$$K_r = K_A K_f \left| \underbrace{\Delta f \cdot \frac{1}{K_f}}_{\Delta SOC_{\text{ref}}} - \underbrace{P_{\text{ref}} \cdot \frac{1}{K_E s}}_{\Delta SOC} \right| = |\Delta f - f_{\text{of}}(s)| \, K_A \tag{17}$$

where K_A is the amplifier gain and f_{ofs} is the offset frequency. In this study, for the reference point corresponding to the frequency is 50 Hz and the BESS power is zero, the offset frequency used for changing the droop characteristic is as follows in Equation (18).

$$f_{\text{ofs}} = \frac{SOC - SOC_{\text{cen}}}{SOC_{\text{tot}}} \left(f_{ofs,\max} - f_{ofs,\min} \right) \tag{18}$$

in which the SOC_{cen} is the center of the SOC range, and in this study, it was chosen to be 50%.

Observing from Equation (17), it can be noted that the primary droop gain is linearly proportional to the absolute value of Δf. This also means that the converter output power in Equation (14) is proportional to the square of Δf, and the reference power is also limited by the real-time power as $P_{max} = U_{PCC}\, I_{dmax}$, in which U_{PCC} is the voltage magnitude at PCC and I_{dmax} is the maximum current of the d-axis.

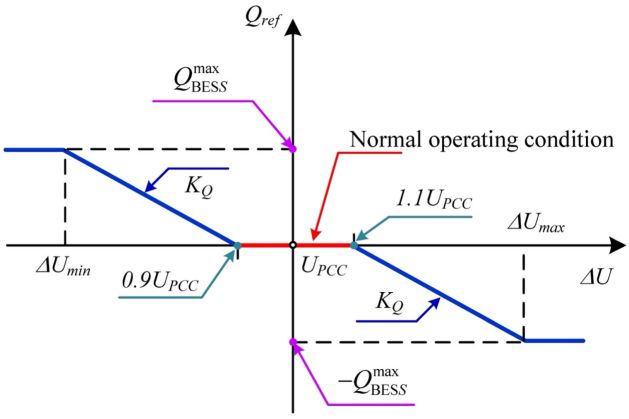

Figure 6. Reactive power–voltage droop characteristics

3.2. Reactive power–voltage droop control

When the power system operates under weak grid conditions, non-synchronous technologies are needed to manage voltage through reactive power control after abnormal voltage fluctuations occur. The amount of reactive power injected or absorbed by the BESS device in response to a given voltage change must comply with grid code requirements. The reference reactive power control signal is generated based on the voltage error between the voltage at PCC and the reference voltage, following the droop control method. In this study, the droop control method was applied from the perspective of the Australian Energy Market Operator (AEMO), and the droop characteristic of voltage variation corresponding to reactive power is shown in Figure 6. The reference reactive power control signal can be obtained as follows in Equation (19):

$$Q_{ref} = \frac{1}{K_Q} \left(U_{ref} - U_{PCC} \right) \tag{19}$$

where U_{ref} is the reference voltage, and K_Q is the reactive power–voltage droop parameter. As shown in Figure 6, the normal operating condition is the voltage deviation between 0.9 U_{PCC} and 1.1 U_{PCC}. In this study, for each 1% voltage drop, 4% of the reactive power was injected into the grid, and for each 1% voltage rise, 6% of the reactive power was absorbed into the grid. The BESS was activated to inject or absorb the reactive power into or from the grid when U_{PCC} was at a value smaller or larger than its values of 90% or 110%, respectively. In case the voltage deviation is less than $\Delta U_{\min}$, then the BESS was injected into the grid with $Q_{\max}$ corresponding to the capacity of the BESS-converter; otherwise, the BESS was absorbed from the grid with $Q_{\max}$ when the voltage deviation is greater than $\Delta U_{\max}$.

3.3. The active and reactive powers control loop

The control strategy based on the d-axis is shown in Figure 5, which includes the first-order filter, the PI controller, and the lead-lag controller. The error between the reference power obtained from Equation (15) and the measured BESS active power at the PCC is passed through the filter. The error between the output of this filter and theΔI_d signal from the charge controller is then passed through the PI controller. The output signal from the PI controller is processed through the lead-lag compensation, washout, and limiter blocks in sequence. The resulting output signal, denoted as $I_{d\_p\_ref}$, was used as the input signal to the battery charge controller. In this paper, the BESS was designed to reduce oscillations by absorbing excess energy and providing additional energy during transient oscillations to minimize

transient energy shortages. This process is entirely dependent on the charging and discharging of the battery, controlled by limiting the battery's SOC level. Therefore, the output signal of the battery charge controller can be obtained based on the following conditions in Equation (20):

$$i_d = \begin{cases} i_{d\_p\_ref} & \text{if } SOC_{\min} \le SOC \le SOC_{\max} \\ 0 & \text{otherwise} \end{cases} \quad (20)$$

where the battery charging and discharging operations are carefully managed to maintain the SOC within the optimal range of $SOC_{\min}$ and $SOC_{\max}$.[33] In this study, $SOC_{\min}$ and $SOC_{\max}$ were selected at 10% and 100%, respectively.[34] The I_d signal was passed through the current limiter to regulate the reference active current in the d axis of I_{d_ref}, which is limited by the maximum current value of the absolute. The difference between the current of I_{d_ref} and the current of I_d is that the feedback signal of ΔI_d was considered the input signal of the active power control loop.

On the contrary, the control strategy based on the q-axis is shown in Figure 6 using the reactive power control loop. It is the same as the active power control loop; the first-order filter, PI controller, and lead-lag controller were considered. The error between the obtained reference reactive power from Equation (19) and the measured BESS reactive power at PCC is passed through the filter. The error between the output signal of this filter and the ΔI_q signal from the charge controller was passed through the PI controller. The output signal from this PI controller was passed through two lag and lead compensations, a washout, and a limiter block, respectively. Then, the output signal denoting I_q WAS passed through the current limiter to regulate the reference active current in the q-axis of I_{d_ref}, which is limited by the maximum current value of the absolute. The difference between the current of I_{q_ref} and the current of I_q to be the feedback signal of ΔI_d was considered the input signal of the reactive power control loop.

The grid input capacity of BESS depends on the DC/AC converter capacity. Therefore, the total current on the d- and q-axes must be equal to the DC/AC converter's rated value to avoid overloading it. The limit between the obtained reference d- and q-axes currents is determined as follows in Equation (21):

$$\begin{cases} I_{d\_ref} = \int_{-|I_{\max}|}^{|I_{\max}|} (I_d)\, dt \\ I_{q\_ref} = \int_{-|I_{\max'}|}^{|I_{\max'}|} (I_q)\, dt \end{cases} \quad (21)$$

where I_{max} is selected equal to 1 per unit and $I_{\max'}$ is determined as follows in Equation (22):

$$I_{\max'} = \sqrt{\int_0^{|I_{\max}|^2} \left(|I_{\max}|^2 - I_d^2\right) dt} \quad (22)$$

3.4. The current controller

The main purpose of the applied current controller in BESS is to regulate reactive and active powers. Its structure is demonstrated in Figure 5. From this figure, the I_{ds} and I_{qs} measured currents at the PCC. The voltage angle at PCC is determined using the phase-locked-loop to calculate I_{ds} and I_{qs} of the d and q reference frame from the abc global reference frame. The error between the I_{d_ref} and I_{q_ref} reference currents from the damping controller and the I_{ds} and I_{qs} measured currents are passed through the PI controller to create the d- and q-axes modulation indexes of m_d and m_q, respectively, which were the input of the PWM.

4. Displayed mathematical equations

4.1. Introduction to test systems

The feasibility of the proposed BESS control method for frequency stability, particularly with high levels of renewable energy, was evaluated using both the IEEE 39-bus system and the Vietnamese Tay Nguyen 500/220 kV system. In the modified IEEE 39-bus system, as shown in Figure 7, three synchronous generators at buses 2, 25, 29, and 23 were replaced with three solar farms (PV1, PV2, and PV3) and one wind farm, with rated powers of 250 MW, 1200 MW, 600 MW, and 1,000 MW, respectively. Details are provided in Table 1. For the Vietnamese Tay Nguyen 500/220 kV system, depicted in Figure 8, it is projected that by 2025, the total generating capacity in the area will reach 5521.5 MW. Of this, 4255.5 MW will come from renewable sources, including 2435.5 MW from PV and 1820 MW from wind turbine generators. Thus, renewable energy will account for approximately 77% of the region's total electricity generation.

The models for the PV and WT systems are based on previous studies.[26,35,36] All dynamic models in the system, such as those for the synchronous generators, excitation systems, transmission lines, and loads, are implemented using the DIgSILENT PF simulation environment. The reference response was evaluated through time-domain simulations conducted in DIgSILENT PF 2021. The parameters for the IEEE 39-bus system were sourced from Thanh et al.,[37] while the parameters for the Vietnamese Tay Nguyen 500/220

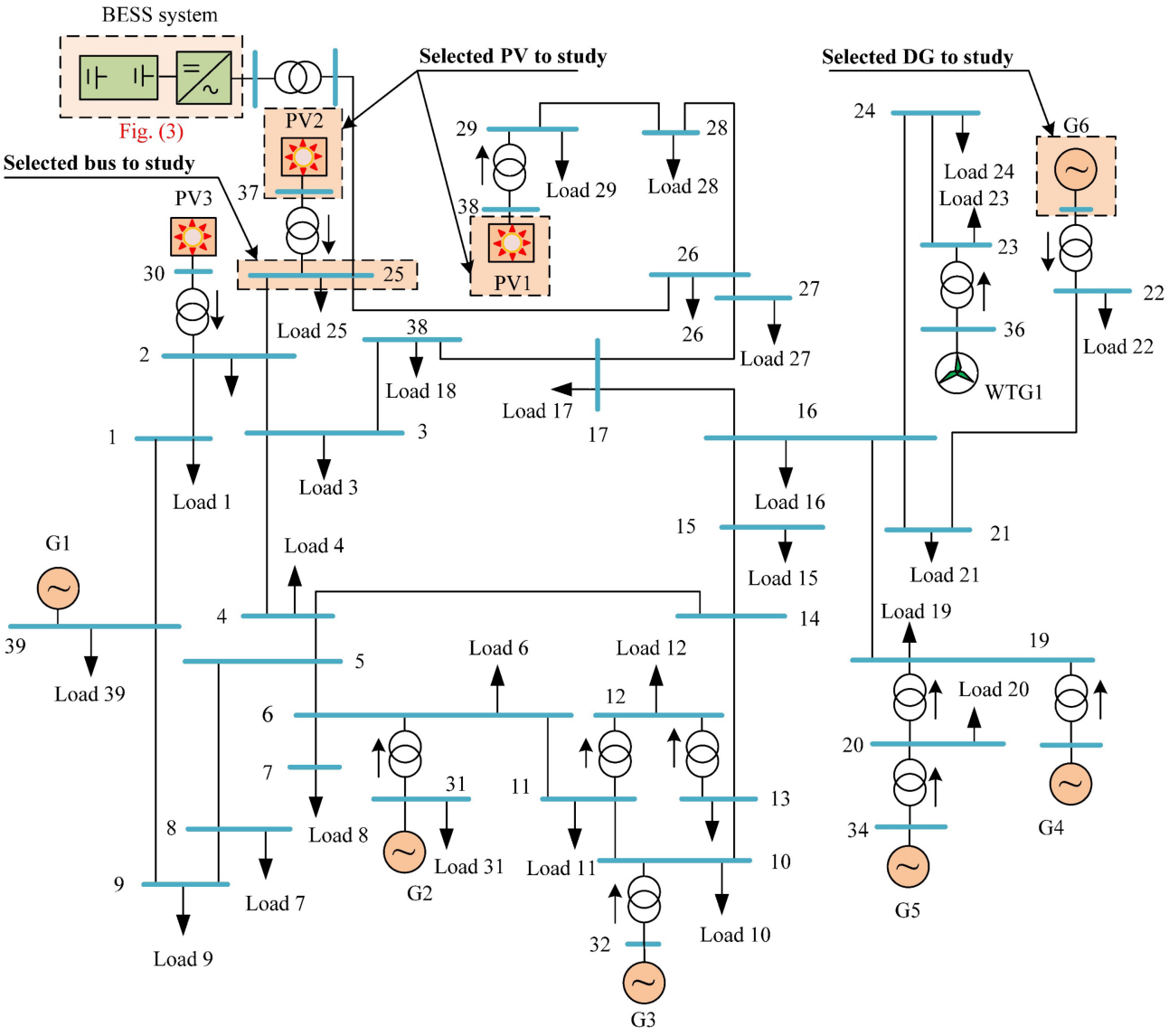

Figure 7. The modified IEEE 39-bus system integrating solar farms, wind farms, and the battery energy storage system

kV system were provided by the Vietnamese National Load Dispatch Center.

The BESS model was developed from the original BESS model in the DIgSILENT PF application manual. The control system has been modified to align with the objectives of this research, and all parameters for the proposed control method, as shown in Figure 5, are listed in Table 2.

4.2. Test case 1: Applying the IEEE 39-bus system

For this case, the simulation was performed based on consideration of two scenarios as follows:

(i) Large cloud cover that can vary the intensity of solar energy radiation and cause significant fluctuations in the output power of the two solar farms of PV1 and PV2.

(ii) Generator G6, with a capacity of 650 MW, experiences a fault and trips out of the power system.

4.2.1. Scenario 1

This case is considered unfavorable. The PV1 and PV2 power plants suddenly reduced their output to the grid due to cloud cover affecting the solar system for a period of 50 s. The sudden loss of a large amount of solar-powered capacity in such a short period can significantly impact the system and cause frequency fluctuations. As shown in Figure 9a, solar radiation drops sharply from 907 to 77 W/m^2 during the cloud cover within 20 s. After the clouds disperse, solar radiation recovers and jumps back to 998 W/m^2 as the sky clears and the plants return to stable operation. This scenario represents a negative situation inspired

Table 1. Power distribution of the generating sources in the modified IEEE 39-bus system

Buses		**2**	**6**	**10**	**19**	**20**	**22**	**23**	**25**	**29**	**39**
Generators	Name	PV3	G2	G3	G4	G5	G6	WT1	PV2	PV1	G1
	Power (MW)	250	527	650	632	254	650	600	1200	600	1000
The total generating capacity of the system: $\sum P_{sys}$ (MW)										6363	
The total generating capacity of PV and WT: $\sum P_{PV+WT}$ (MW)										2650	
The total load of the system $\sum P_{load}$ (MW)[38]										6097	
The proportion of renewable energy sources connected to the system $\frac{\sum P_{\mathrm{PV+WT}}}{\sum P_{sys}} \times 100\%$										41.65%	

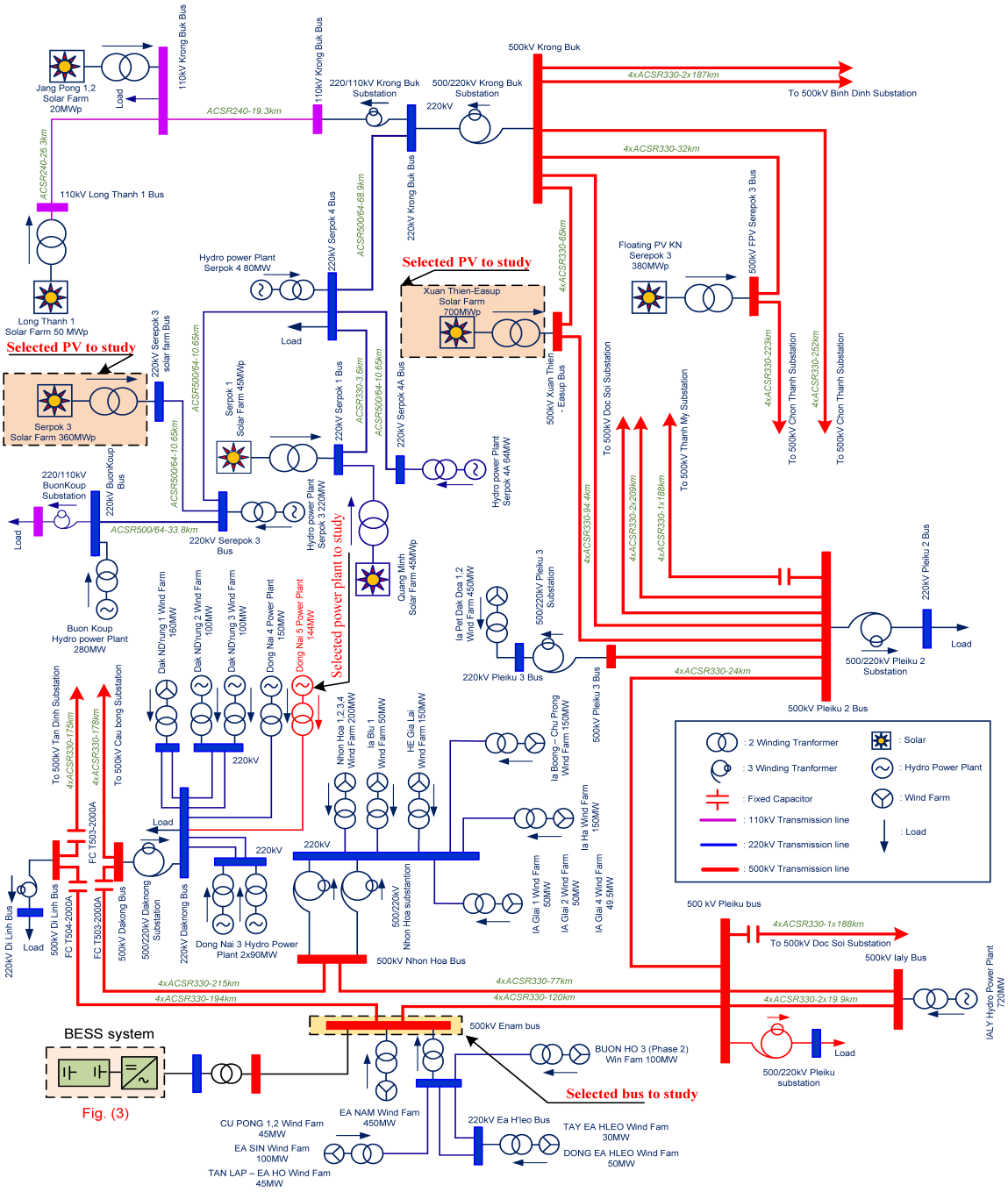

Figure 8. The 500/220 kV Tay Nguyen power system in Vietnam

by a real-life event in Europe, where a significant loss of solar power[39] caused frequency oscillations. The active power output of the PV1 and PV2 solar farms, shown in Figure 9b, decreases significantly when the cloud cover completely obscures the PV1 and PV2 solar farms, resulting

in a drop in solar radiation intensity and corresponding power output. Specifically, at 100 s, the power output of PV1 and PV2 drops abruptly from 500 to 85 MW and from 900 to 333 MW, respectively. At 150 s, the clouds begin to disperse, and the clear sky allows for maximum solar radiation, leading to an increase in power output, which stabilizes at 1542 MW, with PV1 reaching 523 MW and PV2 reaching 1019 MW.

In such a negative scenario, it is evident that the power system's frequency will experience significant oscillations. Figure 10 shows the frequency response at several buses considered most influential to the system. Upon observing this figure, it is clear that the frequency fluctuations at some buses do not meet the grid connection requirements,[40] with bus 25 being the most affected. The frequency of bus 25 reaches 48.6283 Hz, which exceeds the allowed frequency limit of 49 Hz.

4.2.2. Scenario 2

This case involves a sudden lack of generating capacity. The tested IEEE 39-bus system includes Generator 6, which has a capacity of 650 MW and is connected to the nearby PV solar farms. In this scenario, Generator 6 suddenly experienced a fault and tripped out of the power system for a period of 50 s. The frequency of some buses in the system is depicted in Figure 11. Based on this result, it is clear that bus 25 experiences more significant frequency fluctuations than the other buses, with a frequency decrease of 48.6046 Hz, falling below the permissible frequency of 49 Hz.

Thus, in both scenarios, the system's status is at a dangerously unstable level. Therefore, a specific solution is required to improve stability. This paper proposes the installation of the BESS at bus 25. The mathematical modeling and control strategy for the BESS are presented in Section 4, with its control technique and parameters detailed in Figure 6 and Table 2. Additionally, to evaluate the effectiveness of the proposed method, the CBEST method introduced by Yan et al.[34] is also referenced for simulation and comparison.

Figures 12 and 13 show the simulation results for Scenario 1. Figure 12 illustrates the frequency fluctuations on bus 25. As shown, the system frequency drops from 50 Hz when cloud cover occurs. The BESS's active response is shown in Figure 13a, where the BESS generates additional active power for the grid to compensate for the capacity loss caused by cloud cover affecting the PV1 and PV2 solar farms. During this period, the BESS receives the signal and switches from the "no transmission" state to active power transmission, raising the frequency for about 30 s after the fault. The BESS then acts as the primary frequency controller, with a post-fault response time of approximately 1 min. Once the clouds cleared and radiation levels returned to normal, the output power increased due to the excess power transmitted from the BESS to the grid, resulting in a slight increase in system frequency.

Table 2. The parameters of the proposed control method

Parameters	**Value**	**Unit**
1. The active power-frequency control		
K_f	0.0154	-
K_A	4.837	-
K_E	0.219	-
P_{max}	1.0	pu
P_{min}	−1.0	pu
f_{db}	1.0	pu
2. The active power control loop		
T_1^d	11	s
T_2^d	0.7	s
T_3^d	0.3	s
T_4^d	0.2	s
T_5^d	0.1	s
T_6^d	0.4	s
T_w^d	10	s
$K_{p\_1}^d$	100	-
$K_{i\_1}^d$	46	-
$I_{d\max}$	1.0	pu
$I_{d\min}$	−0.4	pu
$I_{q\max}$	1.0	pu
$I_{q\min}$	−1.0	pu
3. The reactive power control loop		
T_1^q	0.2	s
T_2^q	1.4	s
T_3^q	0.45	s
T_4^q	0.3	s
T_5^q	0.1	s
T_6^q	0.4	s
T_w^q	9.0	s
$K_{p\_1}^q$	2.0	-
$K_{i\_1}^q$	85	-
4. The current controller		
$K_{p\_2}^q$	0.1	-
$K_{i\_2}^q$	10	-
$K_{p\_2}^d$	2.5	-
$K_{i\_2}^d$	200	-
ChargeCur	0.05	pu
$SOC_{\min}$	0.1	%
$SOC_{\max}$	100	%
$AbsCur_{\max}$	1.0	pu
U threshold for I_q preference	0.9	pu

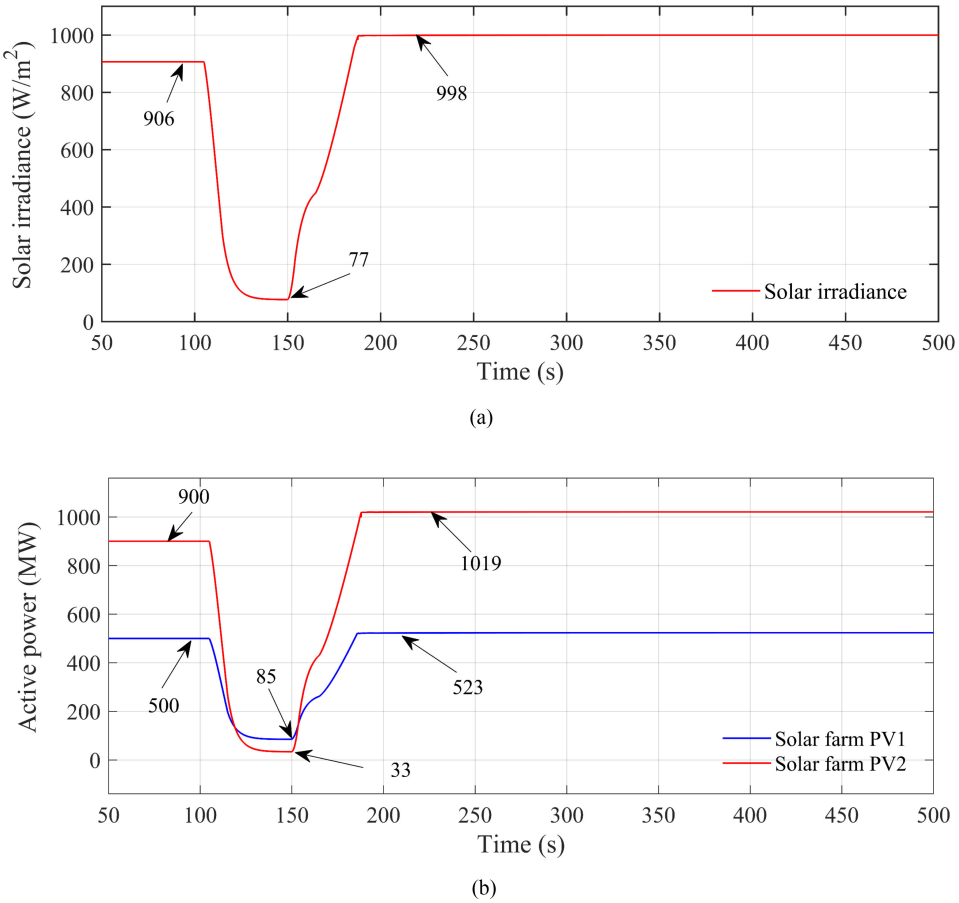

Figure 9. Impact of cloud cover on photovoltaic (PV)1 and PV2 solar farms. (a) Radiation intensity. (b) Output active power

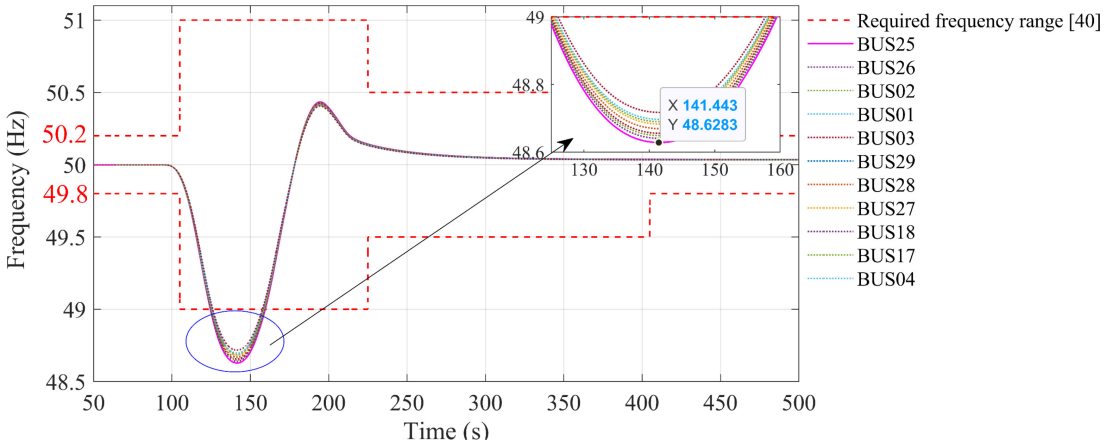

Figure 10. The frequency of some buses in the system is affected by cloud cover, impacting the photovoltaic (PV)1 and PV2 solar farms

The SOC of the BESS is shown in Figure 13b. It demonstrates flexible reserve levels that respond quickly to the system's needs, discharging deep reserves to raise the grid frequency during cloud cover, and rapidly recharging excess energy to stabilize the frequency. This process helps restore the initial reserve level of the BESS system.

The simulation results for Scenario 2 are shown in Figures 14 and 15. Figure 14 illustrates the frequency fluctuations at bus 25. When the time is 100 s, the system is interrupted with a capacity of 650 MW from Generator 6. Without considering BESS, the frequency of 48.86 Hz exceeds the minimum value of 49 Hz, leading to

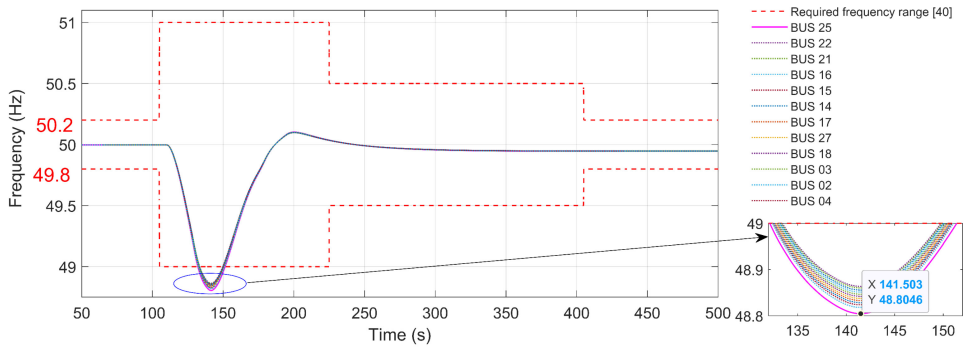

Figure 11. Frequency response at selected buses of the system following the tripping of Generator unit 6, without using the battery energy storage system

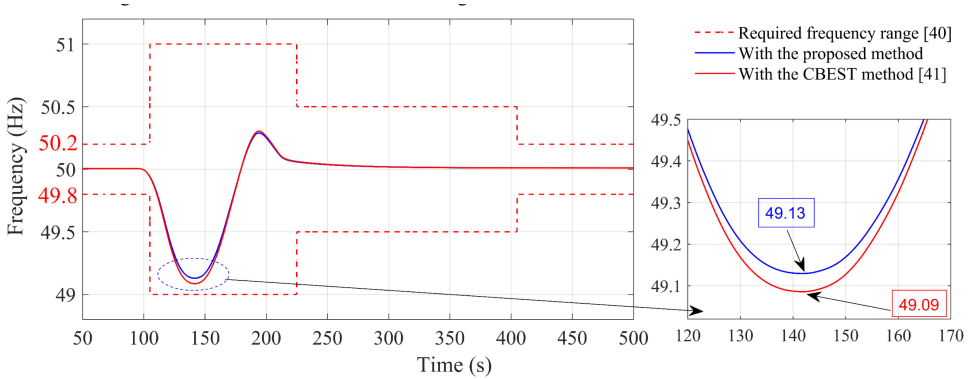

Figure 12. Frequency response at bus 25 of Scenario 1

system instability. The frequency response is improved when the BESS, using the proposed or CBEST method, participates in system frequency regulation. The system frequency drops by approximately 30 s. From 130 to 165 s, the BESS fully provides active power and raises the grid frequency. During this time, the BESS system works under the primary frequency control activated mode. In the period from 165 to 300 s, there is a sharp increase in the grid frequency due to the surplus of active power as generator unit number 6 is reconnected to the grid. At this point, the BESS is responsible for absorbing the excess power and smoothing out the peak, returning the frequency to the stable state. During this time, the BESS system works under the secondary frequency control activated mode. It can be understood that the SOC is recovering. Figure 15 represents the active power of the BESS and SOC. The BESS will increase its active power output in proportion to the frequency deviation. When Generator 6 reconnects, restoring the system's power balance between supply and demand, the BESS will reduce its active power output accordingly.

From the results obtained in Scenarios 1 and 2, the comparison of the frequency response on bus 25 using different methods is summarized in Table 3. It is evident that the proposed method outperforms the CBEST method, as follows:

(i) Frequency response: The proposed method reacts faster when the frequency drops to 49.13 Hz, immediately activating the primary control mode. When the frequency increases, it quickly switches to the secondary control mode, showing better performance than the CBEST method.

(ii) Discharge state: Using the proposed method, the BESS discharges more deeply than with the CBEST method within the same period. This leads to a faster frequency recovery while absorbing more excess active power, bringing the frequency to a steady state.

(iii) Charging state: The BESS responds more quickly and achieves deeper discharge when applying the proposed method compared to the CBEST method. This is primarily because the proposed model tracks the SOC and uses the K_f factor to establish a relationship between the frequency difference and SOC, reducing response time to frequency fluctuations and increasing the BESS's discharge capacity.

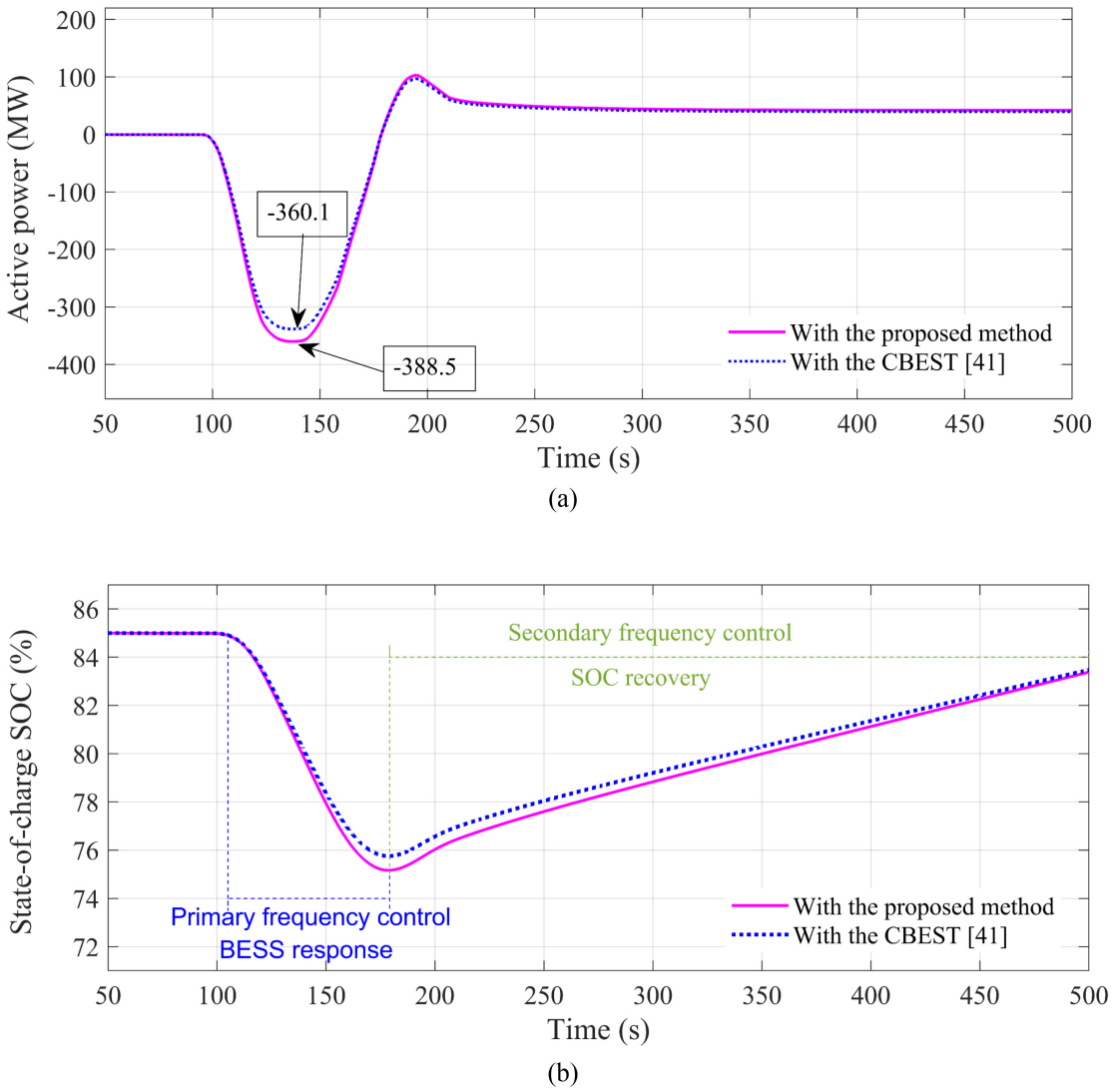

Figure 13. The battery energy storage system (BEES) response for Scenario 1. (a) Active power of the BESS. (b) State-of-charge (SOC) charging status

4.3. Test case 2: Applying the Vietnamese Tay Nguyen 500/220 kV system

After applying the proposed method to the IEEE 39-bus system, its practicality is further evaluated by testing it on the Vietnamese Tay Nguyen 500/220 kV system under the following two scenarios:

4.3.1. Scenario 3

This case is considered unfavorable. Xuan Thien-EaSup and Srepok 3 solar farms suddenly reduced their output capacity to the grid due to the impact of cloud cover on the solar system for a period of 50 s. The sudden loss of a large amount of solar-powered capacity in a short period can significantly impact the system and cause frequency fluctuations. As shown in Figure 9a, the solar radiation drops sharply from 900 to 0 W/m^2 during the cloud cover within 20 s. After the cloud disperses, the solar radiation recovers and jumps back to 1000 W/m^2 as the sky clears and the plants return to stable operation. This scenario assumes a negative situation inspired by a real-life event where Europe experienced a significant loss of solar power,[39] resulting in frequency oscillations. The active power of the Xuan Thien-EaSup and Srepok 3 solar farms, shown in Figure 16, when the cloud cover completely covers the area of the Xuan Thien-EaSup and Srepok 3 solar farms, results in a significant decrease in solar radiation intensity and the corresponding power output. Specifically, at 100 s, the power output of the Xuan Thien-EaSup and Srepok 3 solar farms suddenly drops from 495 to 18.67 MW and from 270 to 10.15 MW, respectively. At 150 s, the clouds start to disperse. The clear sky allows for maximum solar radiation, leading to an increasing power output stabilizing at 867.11 MW, with the Xuan Thien-EaSup solar farm reaching 561.05 MW and the Srepok 3 solar farm reaching 306.06 MW.

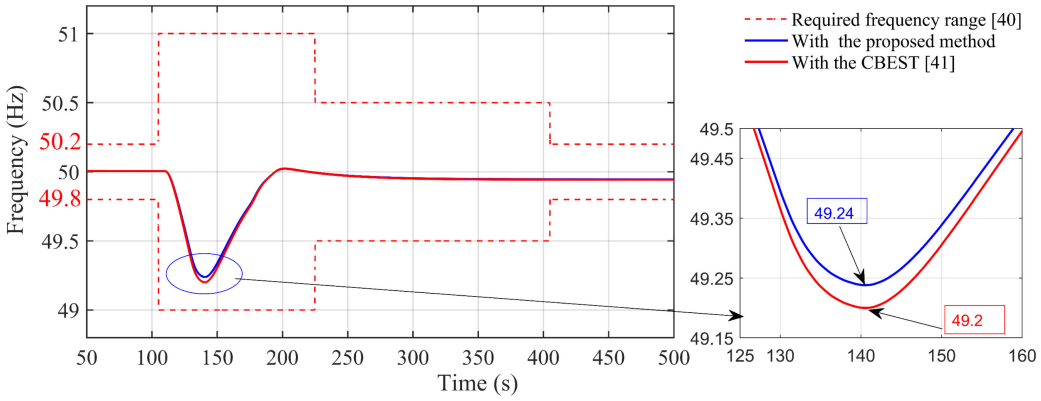

Figure 14. Frequency response at bus 25 of Scenario 2

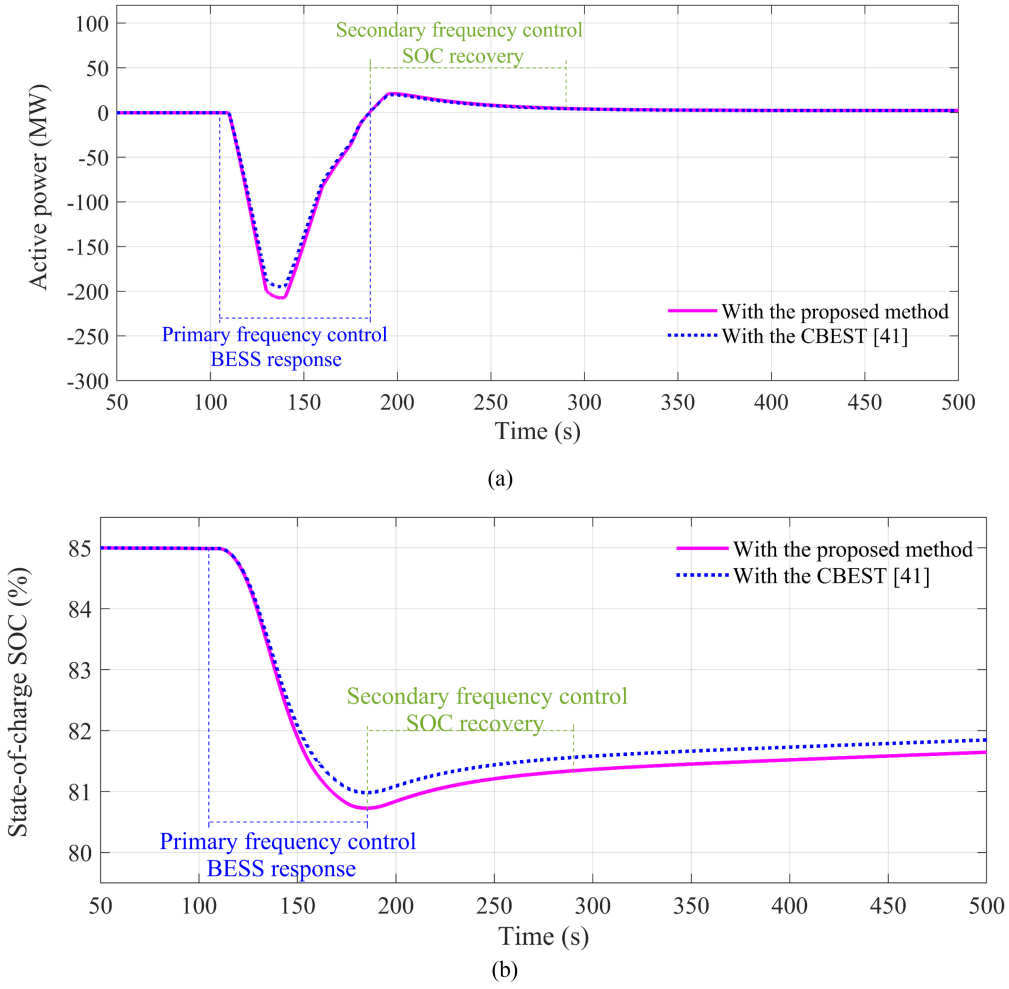

Figure 15. The battery energy storage system (BESS) response for Scenario 2. (a) Active power of the BESS. (b) State-of-charge (SOC) charging status

Table 3. Response on the 25 bus when using different methods

Scenarios	Methods		
	Non-battery energy storage system	**The CBEST method**	**The Proposed method**
1	48.6283	48.09	49.13
2	48.8046	49.20	49.24

With such a negative scenario, it is evident that the power system's frequency will experience significant oscillations. Figure 17a shows the frequency response at some buses considered most influential to the system. Observing this figure, we see that the frequency fluctuations at some buses do not meet the grid connection law requirements,[40] and the most notable is the

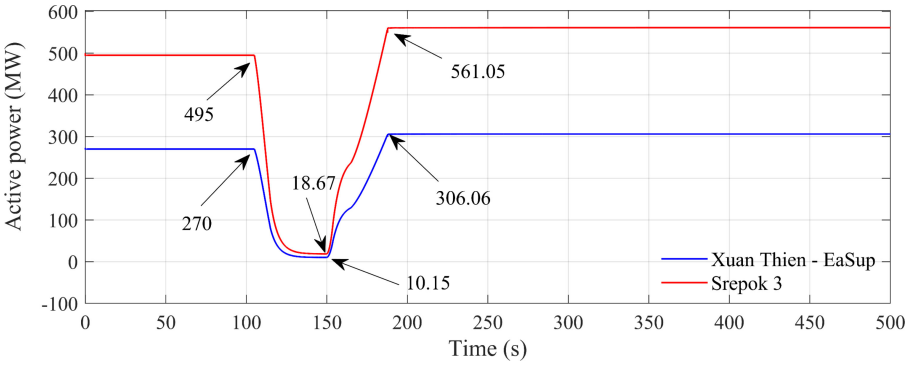

Figure 16. Impact of cloud cover on the output active power of Xuan Thien EaSup and Srepok 3 solar farms

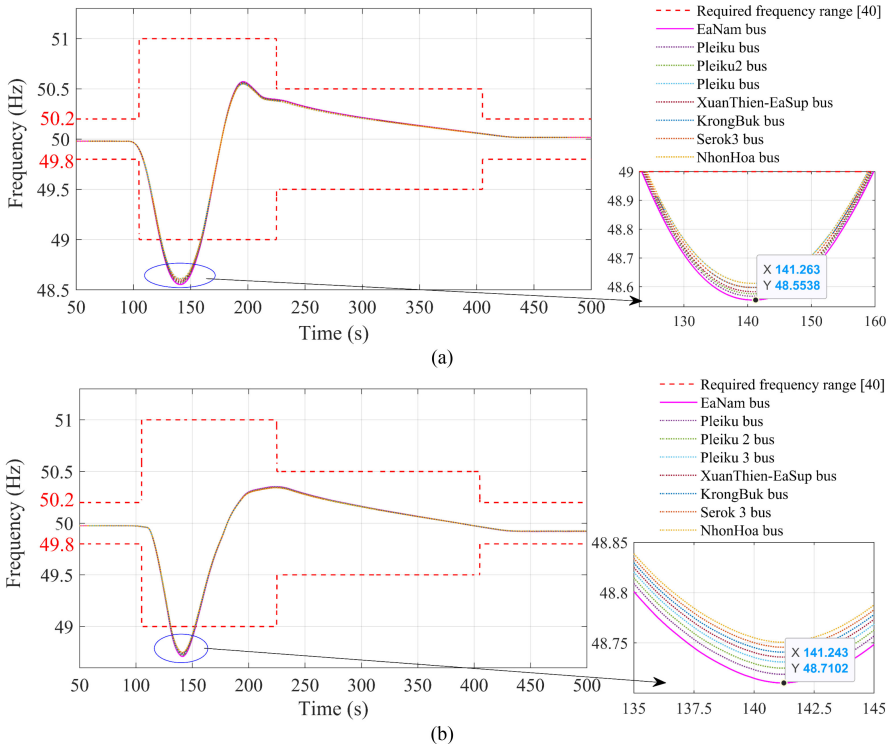

Figure 17. The frequency response at various buses of the system. (a) Scenario 3. (b) Scenario 4

EaNam bus, which is the most affected, with a frequency of 48.5538 Hz, exceeding the allowed frequency of 49 Hz.

4.3.2. Scenario 4

The Dong Nai generator, with a capacity of 144 MW, experienced a fault and disconnected from the power system. The frequency response of several buses in the Vietnamese Tay Nguyen 500/220 kV system is depicted in Figure 17b. Based on the results, the frequency response at the EaNam, Pleiku, Pleiku 2, Pleiku 3, XuanThien-Easup, KrongBuk, Serok 3, and NhonHoa buses failed to meet the requirements set forth in Circular No. 25/2016/TT-BCT, dated November 30, 2016, by the Ministry of Industry and Trade of Vietnam, which regulates the transmission power system.[33] The most notable is EaNam bus, which is the most affected with a frequency of 48.7102 Hz, exceeding the allowed frequency of 49 Hz.

The frequency response at the EaNam bus, comparing the proposed method in this paper with the method introduced by Choi et al.,[41] is illustrated in Figure 18. The results indicate that the frequency response of all buses complies with the grid connection requirements previously outlined.[40] Notably, the EaNam bus exhibits significant improvements in both magnitude and response time. As shown in Figure 18a and b, using the proposed method, the frequency magnitude values are 49.03 and 49.183 Hz, respectively. Employing the method by Choi et al.,[41] the values are 49.07 and 49.143 Hz; and without applying BESS, the values drop to 48.5538 and 48.7102 Hz

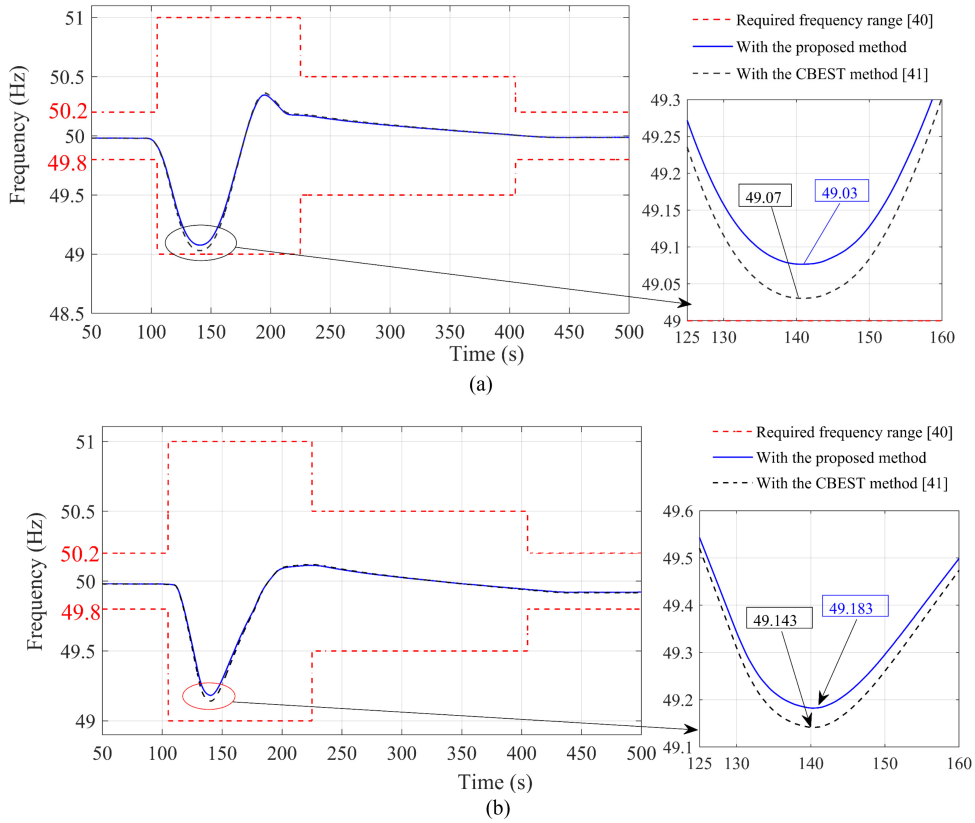

Figure 18. The frequency response at the EaNam bus. (a) Scenario 3. (b) Scenario 4

under Scenarios 3 and 4, respectively. Additionally, the system's restoration time from the moment of the fault is 340 s. The comparison of the frequency response on bus 25 using different methods is summarized in Table 4.

Table 4. Response on the 500 kV EaNam when using different methods

Scenarios	Methods		
	Non-battery energy storage system	**The proposed method**	**The CBEST method**
3	48.5538	49.07	49.03
4	48.7102	49.143	49.183

Observing the results obtained in Scenario 3, the system frequency drops from 50 Hz when cloud cover occurs. The BESS's active response is shown in Figure 19a, where the BESS generates additional active power for the grid to compensate for the capacity loss caused by cloud cover affecting the Xuan Thien-EaSup and Srepok 3 solar farms. During this period, the BESS receives the signal and switches from the "no transmission" state to active power transmission, raising the frequency for about 30 s after the fault. The SOC of the BESS at the 500 kV EaNam bus for Scenario 3 is shown in Figure 19b. It demonstrates flexible reserve levels that respond quickly to the system's needs, discharging deep reserves to raise the grid frequency during cloud cover and rapidly recharging excess energy to stabilize the frequency. This process helps restore the initial reserve level of the BESS system.

In Scenario 4, similar to when the time is 100 s, the system is interrupted with a capacity of 144 MW from the Dong Nai generator. Without considering BESS, the frequency of 48.7102 Hz, as shown in Figure 17b, exceeds the minimum value of 49 Hz, leading to system instability. The frequency response is improved when the BESS, using the proposed or CBEST method, participates in system frequency regulation. The system frequency drops by approximately 30 s, as shown in Figure 18b. From 130 to 165 s, the BESS fully provides active power and raises the grid frequency. During this time, the BESS system works under the primary frequency control activated mode. In the period from 165 to 300 s, there is a sharp increase in the grid frequency due to the surplus of active power as generator unit number 6 is reconnected to the grid. At this point, the BESS is responsible for absorbing the excess power and smoothing out the peak, returning the frequency to the stable state. During this time, the BESS system works under the secondary frequency control activated mode. It can be understood that the SOC is recovering. Figure 20a represents the active

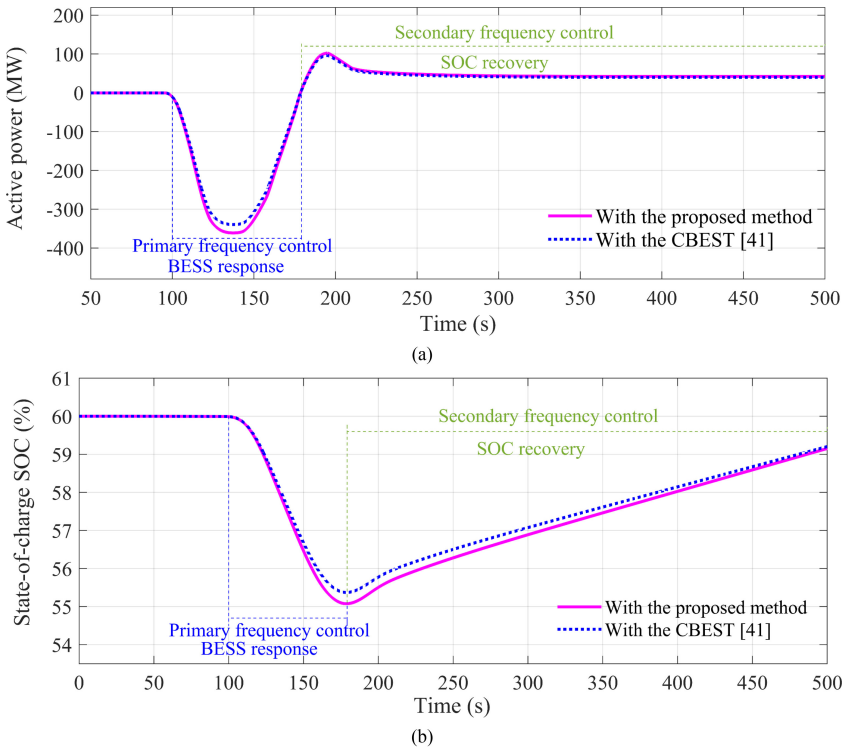

Figure 19. The battery energy storage system (BESS) response at the 500kV EaNam bus for Scenario 3. (a) Active power of the BESS. (b) State-of-charge (SOC) charging status

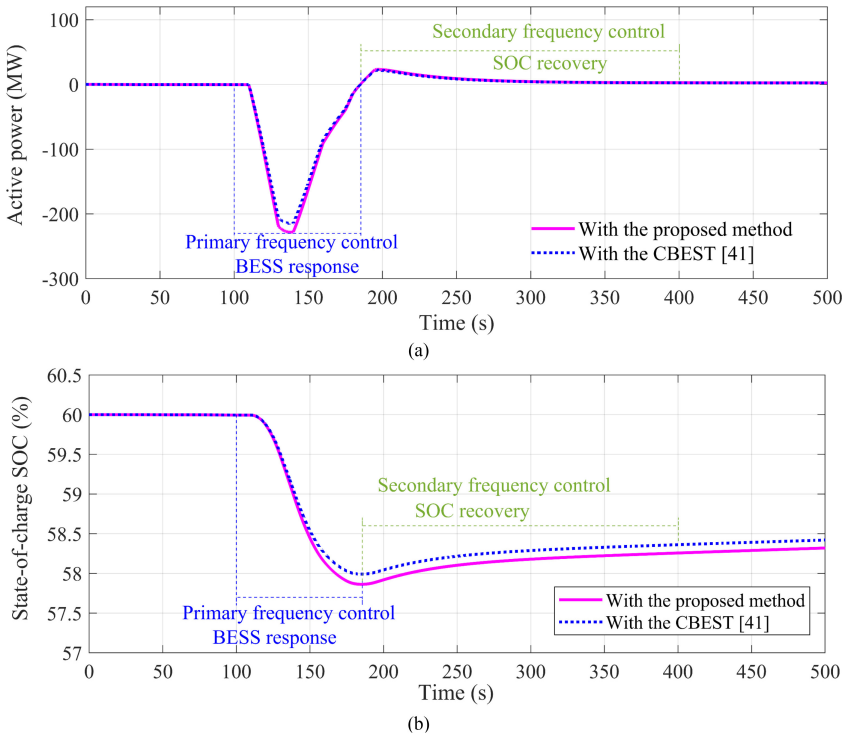

Figure 20. The battery energy storage system (BESS) response at the 500kV EaNam bus for Scenario 4. (a) Active power of the BESS. (b) State-of-charge (SOC) charging status

power of the BESS, and Figure 20b represents the state of the SOC charging status. The BESS will increase its active power output in proportion to the frequency deviation. When the Dong Nai generator reconnects, restoring the system's power balance between supply and demand, the BESS will reduce its active power output accordingly.

Therefore, based on the two testing scenarios for the Vietnamese Tay Nguyen 500/220 kV

system, the proposed BESS control method fully satisfies the power system's flexibility requirements under various conditions and outperforms the CBEST method.[41] Furthermore, this control algorithm enables the BESS to participate in both primary and secondary frequency control, thereby enhancing the stability and efficiency of the power system.

5. Conclusion

This paper proposed a control method for the BESS to support frequency regulation in power systems with a high penetration of RESs. The study analyzed the theoretical foundation of frequency response in power systems from the governance of generators while considering the impact of connected RESs. Based on this analysis, a frequency regulation strategy for the BESS was designed to limit the maximum frequency deviation and improve the maximum RoCoF. The proposed strategy was implemented using a direct-current vector control method within a nested-loop control structure. The structure integrates controllers for frequency, voltage, reactive and active powers, SOC, and d- and q-axis currents. These controllers collaboratively generated a sinusoidal reference signal for the PWM scheme of the DC/AC converter, ensuring precise and effective frequency regulation.

The effectiveness of the proposed method was validated on the IEEE 39-bus standard system. Simulations were conducted to compare the proposed BESS model with the conventional CBEST model in PSS/E under two scenarios: a sudden loss of generating capacity and a sharp decrease in renewable energy output. The results demonstrated the proposed algorithm's ability to effectively manage the SOC of the BESS, stabilizing system frequency during oscillatory events. Furthermore, the new model exhibited superior performance in terms of rapid response to disturbances, deep charging and discharging capabilities, and timely frequency control compared to the widely used CBEST model.

Acknowledgments

The authors thank the Research and Development Center of Power Engineering Consulting Joint Stock Company 4 (PECC4), Vietnam, for supporting this study. The authors also appreciate the support of the Electric Power System Research Group, Industrial University of Ho Chi Minh City, Vietnam.

Funding

None.

Conflict of interest

The authors declare they have no competing interests.

Author contributions

Conceptualization: Le Van Dai, Le Cao Quyen
Formal analysis: Tran Viet Thanh, Nguyen Huu Hieu
Investigation: Tran Viet Thanh, Le Van Dai, Le Cao Quyen
Methodology: Tran Viet Thanh, Le Van Dai, Le Cao Quyen
Writing – original draft: Tran Viet Thanh, Le Cao Quyen
Writing – review & editing: Le Van Dai, Dinh Thanh Viet

Availability of data

All data analyzed and generated have been included in the manuscript.

AI tools statement

All authors confirm that no AI tools were used in the preparation of this manuscript.

Further disclosure

The paper has been uploaded to a preprint server and can be accessed at https://doi.org/10.21203/rs.3.rs-6172264/v1.

References

1. Tekbıyık-Ersoy N. Modeling the renewable energy development in Türkiye with optimization. *Int J Optimiz Control: Theor Appl.* 2025;15(1):135-152. https://doi.org/10.36922/ijocta.1664
2. Teng F, Mu Y, Jia H, Wu J, Zeng P, Strbac G. Challenges on primary frequency control and potential solution from EVs in the future GB electricity system. *Appl Energy.* 2017;194:353-362. https://doi.org/10.1016/j.apenergy.2016.05.123
3. Teng F, Aunedi M, Pudjianto D, Strbac G. Benefits of demand-side response in providing frequency response service in the future GB power system. *Front Energy Res.* 2015;3:36. https://doi.org/10.3389/fenrg.2015.00036
4. Ippolito MG, Musca R, Zizzo G. Analysis and simulations of the primary frequency control during a system split in continental Europe power system. *Energies.* 2021;14(5):1456. https://doi.org/10.3390/en14051456
5. Alqahtani S, Shaher A, Garada A, Cipcigan L. Impact of the high penetration of renewable energy sources on the frequency stability of the Saudi Grid. *Electronics.* 2023;12(6):1470. https://doi.org/10.3390/electronics12061470

6. Saxena A, Shankar R. Improved load frequency control considering dynamic demand regulated power system integrating renewable sources and hybrid energy storage system. *Sustain Energy Technol Assess.* 2022;52:02245. https://doi.org/10.1016/j.seta.2022.102245
7. Aljarrah R, Fawaz BB, Salem Q, Karimi M, Marzooghi H, Azizipanah-Abarghooee R. Issues and challenges of grid-following converters interfacing renewable energy sources in low inertia systems: a review. *IEEE Access.* 2024;12:5534-5561. https://doi.org/10.1109/access.2024.3349630
8. Yu J, Liao S, Xu J. Frequency control strategy for coordinated energy storage system and flexible load in isolated power system. *Energy Rep.* 2022;8:966-979. https://doi.org/10.1016/j.egyr.2022.02.133
9. Kotb KM, Elmorshedy MF, Salama HS, Dán A. Enriching the stability of solar/wind DC microgrids using battery and superconducting magnetic energy storage based fuzzy logic control. *J Energy Storage.* 2022;45:103751. https://doi.org/10.1016/j.est.2021.103751
10. Naderipour A, Ramtin AR, Abdullah A, Marzbali MH, Nowdeh SA, Kamyab H. Hybrid energy system optimization with battery storage for remote area application considering loss of energy probability and economic analysis. *Energy.* 2022;239:122303. https://doi.org/10.1016/j.energy.2021.122303
11. Divya KC, Østergaard J. Battery energy storage technology for power systems-an overview. *Electric Power Syst Res.* 2009;79(4):511-520. https://doi.org/10.1016/j.epsr.2008.09.017
12. Xie X, Guo Y, Wang B, Dong Y, Mou L, Xue F. Improving AGC performance of coal-fueled thermal generators using multi-mw scale BESS: a practical application. *IEEE Trans Smart Grid.* 2018;9(3):1769-1777. https://doi.org/10.1109/tsg.2016.2599579
13. Kjær PC, Lærke R. Experience with primary reserve supplied from energy storage system. In: *Proc. of 2015 17th European Conference on Power Electronics and Applications (EPE'15 ECCE-Europe)*, Geneva, Switzerland; 2025:1-6. https://doi.org/10.1109/epe.2015.7311788
14. Kawakami N, Iijima Y. Overview of battery energy storage systems for stabilization of renewable energy in Japan. In: *Proc. of International Conference on Renewable Energy Research and Applications (ICRERA)*, Nagasaki, Japan; 2012: 1-5. https://doi.org/10.1109/icrera.2012.6477391
15. Killer M, Farrokhseresht M, Paterakis NG. Implementation of large-scale Li-ion battery energy storage systems within the EMEA region. *Appl Energy.* 2020;260:114166. https://doi.org/10.1016/j.apenergy.2019.114166
16. Gulzar MM, Iqbal A, Sibtain D, Khalid M. An innovative converterless solar PV control strategy for a grid connected hybrid PV/Wind/Fuel-cell system coupled with battery energy storage. *IEEE Access.* 2023;11:23245-23259. https://doi.org/10.1109/access.2023.3252891
17. Taghvaei M, Gilvanejad M, Sedighizade M. Cooperation of large-scale wind farm and battery storage in frequency control: an optimal fuzzy-logic based controller. *J Energy Storage.* 2022;46:03834. https://doi.org/10.1016/j.est.2021.103834
18. Mercier P, Cherkaoui R, Oudalov A. Optimizing a battery energy storage system for frequency control application in an isolated power system. *IEEE Trans Power Syst.* 2009;24(3):1469-1477. https://doi.org/10.1109/tpwrs.2009.2022997
19. Gu Y, Zhuang K, Zhang J, Xie J. Adaptive control strategy for primary frequency regulation of BESS in wind farm. In: *Proc. of 9th Asia Conference on Power and Electrical Engineering (ACPEE)*, Shanghai, China; 2024:623-629. https://doi.org/10.1109/acpee60788.2024.10532512
20. Islam A, Jawad A, Masood N.-A. Optimal dispatch strategy of battery energy storage system in utility-scale photovoltaic integrated grid under variability. *J Energy Storage.* 2024;95:112562. https://doi.org/10.1016/j.est.2024.112562
21. El-Bidairi KS, Nguyen HD, Mahmoud TS, Jayasinghe SDG, Guerrero JM. Optimal sizing of battery energy storage systems for dynamic frequency control in an islanded microgrid: a case study of flinders island, Australia. *Energy.* 2020;195:117059. https://doi.org/10.1016/j.energy.2020.117059
22. Teh J, Lai C.-M. Reliability impacts of the dynamic thermal rating and battery energy storage systems on wind-integrated power networks. *Sustain Energy Grids Netw.* 2019;20:100268. https://doi.org/10.1016/j.segan.2019.100268
23. Maeyaert L, Vandevelde L, Döring T. Battery storage for ancillary services in smart distribution grids. *J Energy Storage.* 2020;30:01524. https://doi.org/10.1016/j.est.2020.101524
24. Das CK, Mahmoud TS, Bass O, et al. Optimal sizing of a utility-scale energy storage system in transmission networks to improve frequency response. *J Energy Storage.* 2020;29:101315. https://doi.org/10.1016/j.est.2020.101315
25. Alsharif H, Jalili M, Hasan KN. Power system frequency stability using optimal sizing and placement of battery energy storage system under uncertainty. *J Energy Storage.* 2022;50:104610. https://doi.org/10.1016/j.est.2022.104610
26. Van Dai L. A novel protection method to enhance the grid-connected capability of DFIG based on wind turbines. *IETE J Res.* 2024;70(2):2047-2063. https://doi.org/10.1080/03772063.2022.2163925
27. Ibn-Mohammed T, Koh SCL, Reaney IM, et al. Perovskite solar cells: an integrated hybrid lifecycle assessment and review in comparison with other photovoltaic technologies. *Renew Sustain*

Energy Rev. 2017;80:1321-1344. https://doi.org/10.1016/j.rser.2017.05.095
28. Okafor CE, Folly KA. Optimal placement of Bess in a power system network for frequency support during contingency. *Energy Rep.* 2023;10:3681-3695. https://doi.org/10.1016/j.egyr.2023.10.017
29. Morren J, Pierik J, De Haan SW. Inertial response of variable speed wind turbines. *Electric Power Syst Res.* 2006;76(11):980-987. https://doi.org/10.20944/preprints201609.0118.v1
30. MathWorks. Battery-Implement Generic Battery Model. [Online]. https://www.mathworks.com/help/sps/powersys/ref/battery.html
31. Farrokhabadi M, König S, Cañizares CA, Bhattacharya K, Leibfried T. Battery energy storage system models for microgrid stability analysis and dynamic simulation. *IEEE Trans Power Syst.* 2017;33(2):2301-2312. https://doi.org/10.1109/TPWRS.2017.2740163
32. Wang Y, Ren B. Fault ride-through enhancement for grid-tied PV systems with robust control. *IEEE Trans Ind Electron.* 2017;65(3):2302-2312. https://doi.org/10.1109/TIE.2017.2740858
33. Akca H, AKTAŞ A. Examination and experimental comparison of DC/DC Buck converter topologies used in wireless electric vehicle charging applications. *Int J Optimiz Control: Theor Appl.* 2024;14(2):81-89. https://doi.org/10.11121/ijocta.1503
34. Yan G, Liu D, Li J, Mu G. A cost accounting method of the Li-ion battery energy storage system for frequency regulation considering the effect of life degradation. *Prot Control Modern Power Syst.* 2018;3(1):1-9. https://doi.org/10.1186/s41601-018-0076-2
35. Van Dai L, Hong Thanh P. A feasible MPPT algorithm for the DC/DC boost converter: an applied case for stand-alone solar photovoltaic systems. *Int J Elect Comput Eng Syst.* 2023;14(6):713-724. https://doi.org/10.32985/ijeces.14.6.11
36. Van Dai L, Li X, Dong TLT, Cao Quyen L. An innovative control strategy to improve the fault ride-through capability of DFIGs based on wind energy conversion systems. *Energies.* 2016;9(2):69. https://doi.org/10.3390/en9020069
37. Thanh TV, Viet DT, Hieu NT. A solution to enhance operational effectiveness of the renewable energy sources and power system transmission lines in Vietnam. In: *Proc. of 6th International Conference on Green Technology and Sustainable Development (GTSD)*, Nha Trang City, Vietnam; 2022:693-699. https://doi.org/10.1109/gtsd54989.2022.9989150
38. Mahmud M, Hossain M, Pota H. Investigation of critical parameters for power systems stability with dynamic loads. In: *Proc. of International Conference IEEE PES General Meeting*, Minneapolis, MN, USA; 2010:1-6. https://doi.org/10.1109/pes.2010.5590220
39. Andersson G, Donalek P, Farmer R, et al. Causes of the 2003 major grid blackouts in North America and Europe, and recommended means to improve system dynamic performance. *IEEE Trans Power Syst.* 2005;20(4):1922-1928. https://doi.org/10.1109/tpwrs.2005.857942
40. No. 25/2016/TT-BCT Regulations on Electricity Transmission System. *Ministry of Industry and Trade Circular, Viet Nam.* November 30, 2016, Available online: https://thuvienphapluat.vn/van-ban/Thuong-mai/Circular-25-2016-TT-BCT-regulations-electricity-transmission-system-339051.aspx.
41. Choi WY, Kook KS, Yu GR. Control strategy of BESS for providing both virtual inertia and primary frequency response in the Korean Power System. *Energies.* 2019;12(21):4060. https://doi.org/10.3390/en12214060

Tran Viet Thanh *is currently working at Power Engineering Consulting Joint Stock Company 4 (PECC4), Nha Trang, Khanh Hoa, Vietnam, and work as Deputy Director of the Department of Research and Development of PECC4. He completed his B.Sc. and M.Sc. Engineering degrees in The University of Danang - University of Science and Technology, Da Nang, Vietnam. Currently, he is pursuing a Ph.D. degree in electrical engineering at the University of Danang. His main research directions include power system stability and calculation, renewable energy applications and energy storage equipment design.*
http://orcid.org/0009-0002-9274-9176

Le Cao Quyen *has been at the University of Danang - University of Science and Technology, Da Nang, Vietnam since 2012. He is currently working as the Doctor of the Faculty of Electrical Engineering at the University of Danang. He is also the current Chairman of directors of Power Engineering Consulting Joint Stock Company 4 (PECC4), Nha Trang, Khanh Hoa, Vietnam. He has rich and deep experience in power network system both in traditional and smart grids, as well as in project planning and management. He received his B.Sc. and M.Sc. Engineering degrees from HCM Bach Khoa University, Vietnam. He completed his Ph.D. at the University of Danang. He has conducted research, provided electrical utilities consultancy, and published over twenty publications on his area of expertise. His research interests are system stability, electromagnetic transient and renewable energy.*
https://orcid.org/0009-0001-6760-0495

Dinh Thanh Viet *has been working as Vice Rector and Associate Professor at Department of Electrical and Electronic Engineering, Faculty of Electrical and Electronic Engineering, Dong A University, Da Nang, Vietnam, Vietnam since April 2024. He worked at the University of Danang from May 1997 to March 2024. Dr. Viet was the Dean of Department of Electrical Engineering, Danang University of Technology (DUT) during 2010-2014. He received PhD degree in Electrical Engineering at Vinnytsia National Technical University, Ukraine in 1997. He was a visiting scholar at Washington State University, USA (2007-2008), Arizona State University USA (2010), Grenoble Institute of Technology, France (2013), University of Oldenburg, Germany (2017), Indiana University (2023). He is the author and coauthor of three books, two patents and more than 100 papers in the field of electric power system, renewable energy and higher education. More than 70 PhD and Master students have graduated under his supervision.*
http://orcid.org/0000-0002-3948-9160

Nguyen Huu Hieu *is currently the Principal of the University of Danang - University of Science and Technology, Da Nang, Vietnam. He received his B.Sc degree at Ecole Centrale de Lyon University, France, major in Generalist Engineer field. In 2008, he completed his Ph.D. Electrical Engineering degree in Joseph Fourier University, Grenoble, France and was awarded the title of Associate Professor Doctor in 2018. In addition to conducting research and teaching at the University of Danang, Dr. Hieu has also authored over 23 scientific articles domestically and approximately 27 scientific articles in prestigious international scientific journals to date. His main research interests are power system design, renewable energy applications, signal transmission and automation.*
http://orcid.org/0009-0005-2332-7510

Le Van Dai *was born in Quang Ngai, Vietnam, in 1978. He received the B.S. and M.S. degrees in electrical engineering from Ho Chi Minh City University of Technology and Ho Chi Minh City University of Technology, Vietnam, in 2003 and 2008, respectively, and the Ph.D. degree in control science and engineering from Hunan University, Changsha, China, in 2016. He is currently a lecturer in electrical engineering at the Industrial University of Ho Chi Minh City, Ho Chi Minh, Vietnam. His current research interests include optimizing, controlling, and integrating renewable energy and advanced technologies in power systems and electrical machines..*
http://orcid.org/0000-0001-9312-0025

An International Journal of Optimization and Control: Theories & Applications
(https://accscience.com/journal/ijocta)